E ISSN NO. 2706-9648

Pakistan Journal of Engineering

Pakistan Journal of Engineering

July 2022, Vol. 2

For online access: www.journal.pec.org.pk

Pakistan Engineering Council, HQs, Islamabad

E ISSN NO. 2706-9648

Preface

The Scientific research outcomes and innovative contributions are better disseminated through technical and research journals. No doubt large number of international and national journals are already in place, nevertheless the quality of a good journal rests with its scope, continuity, indexation and citation. PEC being a regulator and promoter of quality higher engineering education, has a role to play for the promotion of quality research and innovation in the country, especially to support the local industry towards indigenous solutions and technology advancement.

With this intent, PEC has taken initiative to publish this research and technical journal covering engineering and technology domains with emphasis on knowledge advancement and creativity through genuine research. It is a technical journal covering the entire engineering regime including technical, management and policy related topics in all disciplines and sub-sectors of engineering, targeting knowledge advancement and innovative solutions.

The standard procedure of online submission, initial scrutiny, reviewers' engagement, manuscript updation and final decision, have been adopted, followed by approvals for publication. There is a complete system of governance including an Advisory Committee and an Editorial Board, comprising eminent professionals (national and international), besides reviewers from all sectors and both from industry and academia.

Engr Muhammad Najeeb Haroon
Patron-in-Chief
Pakistan Journal of Engineering

E ISSN NO. 2706-9648

Editorial Board

Advisory Board

Disclaimer

In accordance with the Review Policy of this Pakistan Journal of Engineering, these Manuscripts have been peer reviewed by our eminent reviewers and experts after quality check, and considerations shared with the authors by Journal Editorial Board. This disclaimer lets that the research work is authors' original creation and is not copied from any other work, except the portions for which the sources are clearly acknowledged therein. The work contains no violation of any existing copyright, other third party rights or any unlawful statements and does not violate any rights of others, and authors agreed to indemnify Pakistan Journal of Engineering against any claims in respect of the above warranties. Since this work is approved after review and being published in the Pakistan Journal of Engineering, the authors' assigned the copyright including, but is not limited to, the right to publish the work, to reproduce it, and to disseminate it, either alone or collectively with other works or in whatever fashion the Journal considers appropriate. The authors reserve all proprietary rights other than copyright such as patent rights and the right to use all or part of this article in future works of their own such as lectures, reviews, personal websites, text books, etc.

Contents

1. SUITABILITY OF CONCRETE INCORPORATED WITH SCRUBBED RUBBER TIRE PARTICLES: ASSESSMENT BASED ON DESTRUCTIVE AND NON-DESTRUCTIVE TESTING 6

   Raja Bilal Nasar Khan, Anwar Khitab

2. TO STUDY THE MECHANICAL PROPERTY OF CONCRETE BY INCORPORATION OF COCONUT AND GLASS FIBER 23

   Safdar Iqbal, Sajid Ullah, Haris Khan, Beenish Jehan, Farhan Saleh, Major Ahmed Sajjad Amir Sohail

3. IMPROVED GREY WOLF OPTIMIZATION IMPLEMENTED ON ECONOMIC LOAD DISPATCH PROBLEM. 40

   Ali Hassan, Muhammad Awais Ali, Dr. Ashfaq Ahmed

4. EFFICACY OF PHOSPHORUS PENTOXIDE (P2O5) ON THE YIELD OF WHEAT USING FERTILIZER BAND DRILL IN MIXED CROP ZONE OF PUNJAB, PAKISTAN 54

   Muhammad Ansir Muneer, Muhammad Yamin, Qaisar Mehmood, Muhammad Arshad

5. DESIGN OF SOLAR POWERED UNMANNED AERIAL VEHICLE WITH PERPETUAL FLIGHT FOR SURVEILLANCE OF LONG-DISTANCE GAS PIPELINES 62

   Aun Haider

E ISSN NO. 2706-9648

Pakistan Journal of Engineering

For online access, please visit:
journal.pec.org.pk

SUITABILITY OF CONCRETE INCORPORATED WITH SCRUBBED RUBBER TIRE PARTICLES: ASSESSMENT BASED ON DESTRUCTIVE AND NON-DESTRUCTIVE TESTING

Anwar Khitab[*1] *, Raja Bilal Nasar Khan*[2]

[*1] *Professor of Civil Engineering at Mirpur University of Science and Technology, Azad Kashmir, Pakistan.*
[2]*Junior lecturer at Civil Engineering Department, Mirpur University of Science of Technology, Azad Kashmir, Pakistan*

ARTICLE INFO

Article History:
Accepted on 12 January 2022
Published on 25 July 2022

Keywords
Concrete, waste rubber tires, recycling, insulation, lightweight, strength

ABSTRACT

The rubberized crumb concrete has been studied and evaluated by partially replacing sand with crumb rubber. The study aims to present a lightweight and eco-friendly material, that recycles waste tire rubber, and possess insulating character with a marginal compromise over mechanical strength. The replacement levels were kept as 0, 5, 10, and 15%. The workability was checked through standard slump test. The strength was evaluated by standard compressive, tensile, and flexural tests at 3, 7, and 28 days. The microstructure was checked through scanning electron microscopy, and the quality of the material was evaluated through the non-destructive ultrasonic pulse velocity (UPV) test. Results reveal that rubberized concrete exhibits a true slump at all replacement levels, indicating that rubber particles do not affect the overall cohesiveness of the material. Density decreases with rubber content and is linearly related to the UPV values. Compressive strength increases up to 5% replacement level, indicating some mechanical interlocking at lower levels between rubber particles and cement matrix. Indirect tensile and flexural strengths decrease with rubber content and are closely related to density and UPV values. Microscopy reveals that the crumb particles induce voids and possess the bridging capacity for crack retention. Identical formation of CSH gel was observed in both control and rubberized concrete. However, the interfacial transition zone of rubberized concrete was weaker than that of the control one.

1. INTRODUCTION

Concrete is an important building material. The world is constantly on the increase adapting concrete due to its resilient and sustainable nature. According to the census data provided, around 4.4 billion tons of concrete are manufactured annually around the globe [1]. Ordinary concrete comprises three basic ingredients; water, aggregate (rock, sand, or gravel), and cement. Cement and water are chemically reactive ingredients, whereas aggregates must be filler and inert. The materials are mixed in different ratios as per need. Cement and water make fluid cement paste, which hardens with time. This mixture is allowed to set and hardens into a stiff rock-like material [2].

On the other hand, rubber tire production is also high. It is reported that 2.2 billion units are being produced each year; the production is estimated to rise to 2.7 billion by 2022 [3]. It has been analyzed that when one tire expires, it becomes useless for producing other tires and is considered waste [4]. Recycling waste rubber tire is not easy because of its vulcanized nature. Proper disposal is necessary as it threatens the environment. The simplest way of disposing of waste rubber tires is to decompose them either by burning or burying them inside the earth. Burning tires have adverse effects on the environment, whereas burying needs landfills. Construction across the globe is increasing over time, and it accelerates the demand for cement, sand, and aggregates: This, in turn, depletes natural resources like limestone, sand, and clay. The rapid use of these materials needs to slow down for coping with the natural and environmental changes. Frequent use of conventional concrete also necessitates a careful selection of the constituent materials for avoiding undesirable consequences like alkali-silica or alkali carbonate reactions and many others [5–7]. Several research groups have worked aiming at the potential recycling of waste rubber tires in construction materials. In the following paragraph, a brief look at past studies using waste rubber in concrete is presented.

The addition of crumb rubber as a substitute for the air-entraining agent in concrete [8]. They have reported that the addition produces air-entrained concrete with reduced unit weight, compressive and tensile strength. In addition, the rubberized concrete shows a ductile failure. Ho et al. studied the effect of replacing natural sand (percentage of volume) with crumb rubber for concrete pavements [9]. The effect was studied via three-point bending, Brittleness index (BI), Acoustic emission (AE), and Elastic quality index (EQI) tests. The brittleness index indicated that the damage decreased with the increase of rubber content. The acoustic emission test indicated better sound absorption with rubber. The Elastic Quality Index (EQI) revealed that rubberized concrete exhibited EQI values within acceptable limits. Ghedan et al. studied the partial replacement of coarse aggregates by chipped rubber particles treated with and without saline [10]. They have reported a reduced thermal conductivity with rubber aggregates. In addition, they have expressed that saline-treated aggregates recover some of the loss in compressive strength. Pacheco-Torgal prepared rubber particles from waste tires by either ambient or cryogenic processes [11]. Different groups of various dimensions of crumb rubber particles were mixed in concrete. Major classes were shredded / chipped rubber (13 – 73 mm), crumb rubber (0.425 – 4.75 mm) and ground rubber (0.075 – 0.425 mm). They noticed that the sound absorption, vibration absorption, and impact resistance characteristics were better than the control specimens. It was also observed that

sound absorption and resilience against the impact increased as the rubber content in concrete was increased. Thomas et al. performed abrasion test conforming to Indian Standards (IS: 1237-1980) on 28 days cured concrete [12]. Compared to controlled concrete specimens, it was found that rubberized concrete was more resilient against abrasion. The statistical analysis revealed that the quantity of rubber showed a linear positive effect vis-à-vis resistance against abrasion. The weak bonding between the cement paste and the crumb rubber particles did not negatively affect the abrasion resistance of the rubberized concrete. Nevertheless, it adversely affected the compressive strength. Paine et al. cast cubes by replacing sand with crumb rubber particles at different ratios and performed CEN slab test [13]: The rubberized concrete performance was much better under freeze and thaw conditions than traditional concrete. The behavior of crumb rubber and air-entraining agent in concrete was found identical. Zukri et al. studied the combined effect of crumb rubber and steel fibers extracted from waste rubber tires [14]. They have reported that the composite concrete material showed a high probability to be used as an insulating (due to rubber) and reinforcing material (due to steel wires/fibers) for non-structural purposes.

In this research, crumb rubber tire is used as a partial replacement of sand in ordinary concrete rather than as an addition. The novelty of this research lies in the determination of the optimal amount of crumb rubber for replacement with locally available sand. This research particularly focuses on using crumb rubber in concrete made from locally available sand and gravel. The work is intended to preserve our local reserves in accordance to the following sustainable development goals (SDGs) of UNO: SDG No. 11 i.e., Sustainable cities and communities and SDG No. 12 i.e., Responsible consumption and production.

During this study, the replacement levels were kept as 0%, 5%, 10%, and 15%. The intention was: (1) using a simple technique like scrubbing the tires for producing rubber particles of the size of sand (2) recycling waste rubber hence contributing to the preservation of the natural environment, (3) deciding a suitable sand replacement level, keeping in view different physical, chemical and mechanical perspectives, and (4) Saving the natural resources by reduced sand content.

2. MATERIALS AND METHODS

Ordinary and crumb rubber concrete (CRC) specimens were cast using local cement, sand, and coarse aggregates as per standard ASTM C31 procedure [15]. A grade C-53 cement was used, and its chemical composition and physical properties are given in Table 1 and Table 2, respectively. The grade C-53 cement conforms to ASTM type-I cement.

Table 1-Chemical composition of Cement

Components	Percentages
Gypsum	1%
Silica	30%
Iron Oxide	2%
Magnesium Oxide	1%
Aluminum Oxide	5%
Lime	61%

Table 2-Physical characteristics of cement

Color	Grey
Specific gravity	3.15
Normal Consistency(%)	30%
Soundness(mm)	2%
Fineness(%)	1%
Initial Setting time (minutes)	30
Final Setting time(minutes)	610

Lawrencepur river sand was used as fine aggregates: its physical properties are described in Table 3.

Table 3-Physical properties of sand

Specific Gravity	2.69
Fineness Modulus	2.72
Bulk Density (Kg/m^3)	1500
Dry rodded Bulk Density(Kg/m^3)	1850
Water absorption(%)	3.88
Water Content (%)	2.01

Coarse aggregates were acquired from the limestone quarry of Margalla near the capital Islamabad, and its characteristics are shown in Table 4. The selected quarries are well-documented, tested, and contain inert materials. All constituents were carefully decided to avoid any unfavorable consequences, as mentioned above.

Table 4- Physical properties of coarse aggregates

Max. size (mm)	19
Specific Gravity	2.48
Bulk Density(kg/m^3)	1598
Dry rodded density(kg/m^3)	1610
Water absorption(%)	1.49
Void(%)	34.11
Impact Value(%)	13.20
Crushing Value(%)	28.20

Crumb rubber was produced in the laboratory by shredding the waste tires and scrubbing them with sandstone. The finished product is shown in Fig 1. The physical properties of crumb rubber are mentioned in Table 5.

Fig 1 Crumb Rubber

Table 5- Physical properties of crumb rubber

Specific Gravity	1.66
Color	Black
Surface	Moderately rough
Fineness Modulus(%)	4.1
Water absorption(%)	1.25

Comparing Tables 3 and 5 shows that crumb rubber should result in lightweight finished products owing to lesser specific gravity. Crumb rubber contains coarser particles and has lesser water absorption. Low water absorption values add to the quality of concrete. Sieve analysis of sand and sand-crumb rubber mix as per standard ASTM C136 method [16] is shown in Fig 2. All mixes are within limits, defined in ASTM standards for fine aggregates (5). Nevertheless, the results show a slightly coarser mix (compared to sand) in all cases.

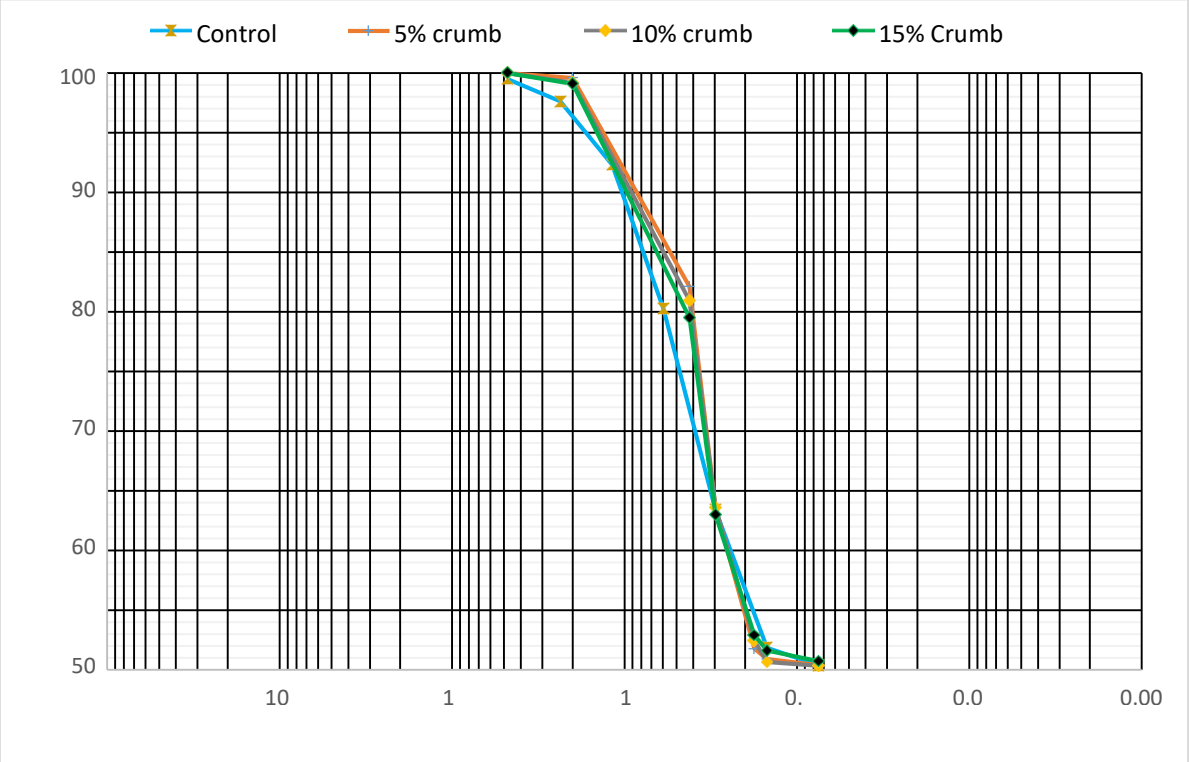

Fig 2 Particle size analysis of fine aggregates mixes

A thorough mix design was prepared for both the control units (C0) and the modified units (partially replaced sand) with notations as C5, C10, C15.

The composition of the mixes is shown in Table 6.

Table 6- Concrete Compositions

Sample	Mix Design	W/C ratio	Cement (kg/m^3)	Sand (kg/m^3)	Crumb Rubber (kg/m^3)	Coarse Aggregate (kg/m^3)	Water (Liters)
(C0)	1:1.56:3.12	0.45	11	17.16	0	34.32	4.95
(C5)	1:1.56:3.12	0.45	11	16.302	0.858	34.32	4.95
(C10)	1:1.56:3.12	0.45	11	15.44	1.716	34.32	4.95
(C15)	1:1.56:3.12	0.45	11	14.586	2.574	34.32	4.95

The samples after mixing were cast using ASTM C31 standards(15). The molds were lubricated properly by applying diesel oil and were thoroughly cleaned by using sandpaper. The Casting was done in three layers. Each layer was tempted 25 times. The molds were removed after 24hrs, and the specimens were marked by date of casting as an identity and then were put inside the curing tank having clean potable water.

After casting, fresh specimens were tested against workability and fresh density following ASTM standard methods C143 and C138, respectively [17,18]. After the curing period, mechanical properties were determined as per standard ASTM procedures [19-21]. Ultrasonic pulse velocity was determined as per ASTM C597-09 method [22]. The microstructures were examined through Scanning Electron Microscopy.

3. RESULTS AND DISCUSSION

3.1 Workability

The slump test is shown Fig 3**.** A true

slump was observed in all the fresh specimens, regardless of rubber quantity: All concrete specimens were observed to recede evenly, maintaining the mold shape. True slump is the most desirable and indicates the cohesiveness of the concrete (5).

Fig 3 Slump test of CRC containing 10% rubber content

The results show that rubberized concrete is generally cohesive. The slump values are shown in Table 7.

Table 7-Variation of slump with rubber content

Specimen	Slump (mm)
Co	48
C5	40
C10	31
C15	22

ACI 211.1-91 codes designate 25 mm as the minimum slump for ordinary concrete works [23]:All specimens except C15 qualify the essential requirement for the slump of ordinary works. From the results, it is clear that the workability decreases with rubber content. The slump is medium from 0-5% replacement, while higher replacement levels result in low-workability concrete. The loss of workability in CRC is generally attributed to the higher absorption rate of rubber particles [24-25]. At the same time, it also depends on the degree of compaction: Higher compaction factor leads to higher workability and vice versa [26]. The slump test involves rodding in three layers. Due to its shock-absorbing characteristics, the rubber particles hinder the exclusion of voids, which reduces workability. This effect was latterly confirmed in the concrete surface view given in Fig. 7 and the microscopic view in Fig. 12.

Density

Fresh densities of the specimens are mentioned in Table 8. ACI 211.1-91 codes report 2350 kg/m^3, as the first estimate of fresh concrete density with maximum 19 mm size aggregates [23]: As such, all specimens except C15 have fresh density more than that specified by ACI codes.

Table 8-Variation of fresh density with rubber content

Specimens	Density(Kg/m^3)
Co	2512
C5	2414
C10	2365
C15	2305

The results reveal that the density decreases with an increase in rubber content. The effect is attributed to the lower specific gravity of the rubber content compared to sand and the induction of voids, as observed through the surface and microscopic view. The results align with the previous studies, where partial replacement by lighter materials results in lower densities and increased porosities [27]. Nevertheless, low-density materials are helpful, as they reduce the dead weight of the structures and, owing to lower thermal conductivity, lessen the energy requirement of the buildings [28,29].

3.2 Mechanical properties

3.2.1 Compressive strength

Compressive strength results are presented in Table 9. It indicates that the strength increases up to 4% at 5% replacement and then gradually decreases. The increase in compressive strength at the lower replacement level of sand by crumb rubber is mentioned in the literature without any reasoning [30].

Table 9-Variation of compressive strength (MPa) with rubber content

Notation	3 Days	7 Days	28 Days
C0	10.49	18.21	28.13
C5	11.30	19.85	29.63
C10	10.96	17.29	26.33
C15	10.28	14.93	22.51

At 5% replacement, the effect of the rough texture of rubber particles providing mechanical friction with surrounding cement paste seems dominant (Refer to Fig 10 and Fig. 11). As the rubber content increases, other factors govern the strength, like poor compaction and induction of voids: at higher content, uniform distribution of rubber content is also a problem, and the rubber particles were observed to form lumps (agglomeration). The decrease in compressive strength with increasing rubber content agrees with the previous studies (31,32).

The crack pattern of C5 was highly ductile as compared to that of C0. On the other hand, concrete spalled when C10 and C15 were tested: spalling and ductile behavior are shown in Fig 4 and Fig 5, respectively. The spalling of concrete is attributed to a weaker rubber-cement interface. However, in all the cases of CRC, the failure starts from a hairline crack, which gradually increases in size: This is an indication of ductile behavior.

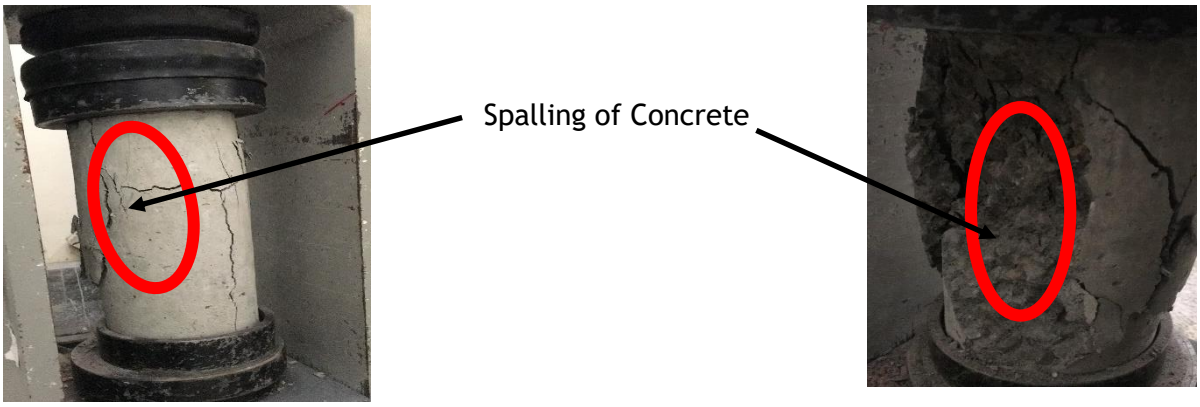

(C10) (C15)

Fig 4 Crack pattern in concrete specimens containing 10 and 15% partial replacement of sand by crumb rubber

Fig 5 Initialization of cracks in crumb rubber concrete

The surface textures of all the specimens are shown in Fig. 7. It is evident that as the rubber content increases, it becomes more and more challenging to achieve proper compaction. This, in turn, increases voids. The results necessitate the use of special compaction techniques to cope with increasing voids quantities. The techniques include but are not limited to (1) Vibropressing, (2) Joilting, (3) Centrifugation, (4) Air jets (33). The appropriate method can be selected depending upon the field conditions and requirements.

3.3.2 Tensile strength

The results of the split cylinder tensile strength are shown in Table 10.

Table 10-Variation of Split cylinder tensile strength (MPa) with rubber content

Specimen	3 Days	7 Days	28 Days
C0	1.8	1.96	2.38
C5	1.94	2.07	2.22
C10	1.83	2.03	2.19
C15	1.66	1.80	2.04

It can be seen that the split tensile strength decreases with rubber content. At three days, the strength increases with an increase in rubber content up to 5% replacement and gradually decreases. The same trend was observed at seven days. However, at 28 days, the strength continuously decreases with an increase in

rubber content. According to Singh et al., the tensile strength of concrete largely depends on the paste quality and that of its interfacial transition zone [34]. While cement paste quality is observed unaffected, the ITZ of rubberized concrete is highly porous (Fig. 12). In literature, the tensile strength of concrete is considered a function of compressive strength [35], yet its deviation from the trend of compressive strength in special concretes is never out of the question [36].

3.2.2 Flexural strength

The summary of the results for flexural analysis is shown in
Table . Just like the above two tests, the flexural strength also decreases with rubber content. The decline in flexural strength in concrete is attributed to a loss in density, weaker bonds, and increased voids. However, the crack pattern of crumb rubber concrete was ductile: slight hairline cracks were seen initially, and the failure was slightly gradual compared to those with no crumb rubber.

Table 11 -Variation of flexural strength with rubber content

Notation	3 Days	7 Days	28 Days
C0	3.45	6.07	7.62
C5	2.76	5.70	6.97
C10	2.50	4.60	6.27
C15	2.39	4.41	5.43

The initialization of cracks during the flexural test is shown in Fig 5. Like other fibers, the rubber particles can also produce a crack bridging effect, as shown in Fig 6.
According to Sadeghbeigi, flexural strength is a measure of the bond strength of the material. In contrast, compressive strength is more related to particle size and packing/filling (37): that highlights the reasons, where compressive strength increases up to 5% replacement, flexural strength decreases with an increase in rubber content beyond 0%.

Fig. 6 Chunks of concrete bridged via crumb rubber

3.3 Ultrasonic pulse velocity

The summary of the ultrasonic pulse velocity test is shown in Table 12. Rubber content generates voids and hinders the pulse wave path, resulting in a decrease in pulse velocity. The production of voids can be seen in the microscopic view shown in Fig 12. The results are in close coordination with the mechanical strength test results shown in Table 9, 10 and 11 and surface textures shown in Fig 7.

Table 12-Variation of ultrasonic pulse velocity (km/s) with crumb rubber

Notation	UPV
C0	3.5
C5	2.9
C10	2.45
C15	2.1

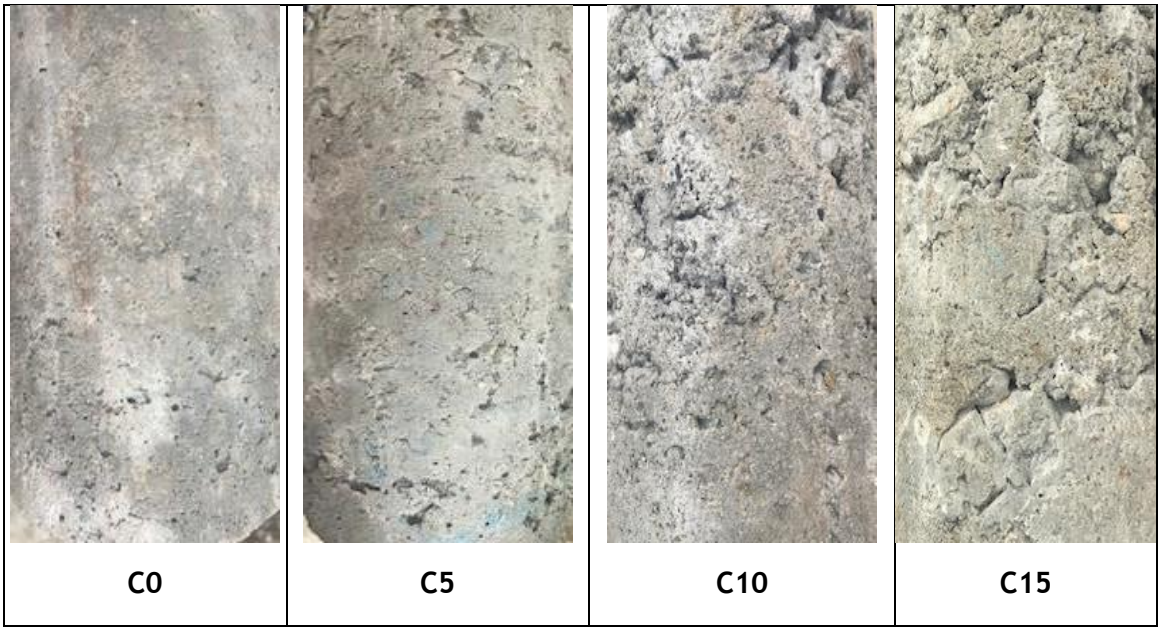

Fig 7. Deterioration of surface texture with increasing rubber content

According to Singh, the ultrasonic pulse strongly depends on concrete density (34). As the density given in Table reduces with an increase in rubber content, the decrease in UPV is quite understandable. The linear variation of UPV with change in density is shown in Fig 8.

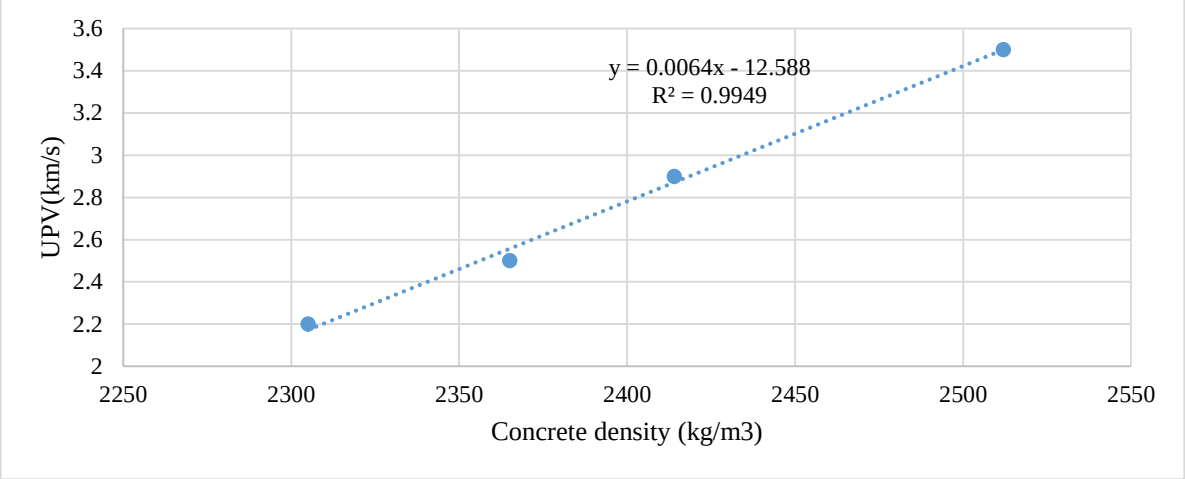

Fig 8. Variation of UPV as a function of concrete density

3.4 Microscopic analysis

The nature of concrete shows that it is a heterogeneous material (38). SEM analysis was performed to investigate the presence of bonding characteristics of crumb rubber and hydrated cement paste. The cores of proper size with a diameter of 2 inches (50 mm) were taken from samples after 28 days of curing, adequately dried, placed into the vacuum for 24hrs and sent for SEM examination. The cores of each sample are shown in Fig 9.

Fig 9 Concrete cores for SEM analysis

Fig 10 and Fig 11 show the SEM images of the specimen with 5% replacement of sand by rubber particles. The rubber particles have an irregular shape with flakiness, rough texture, and undulations.

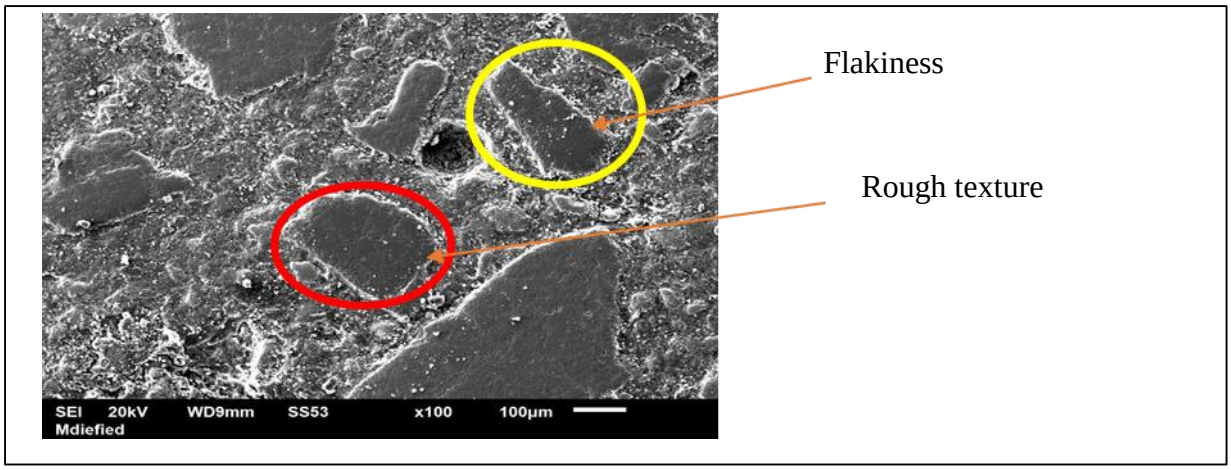

Fig 10 Microscopic view showing the texture of rubber particles in cement matrix at 5% replacement level

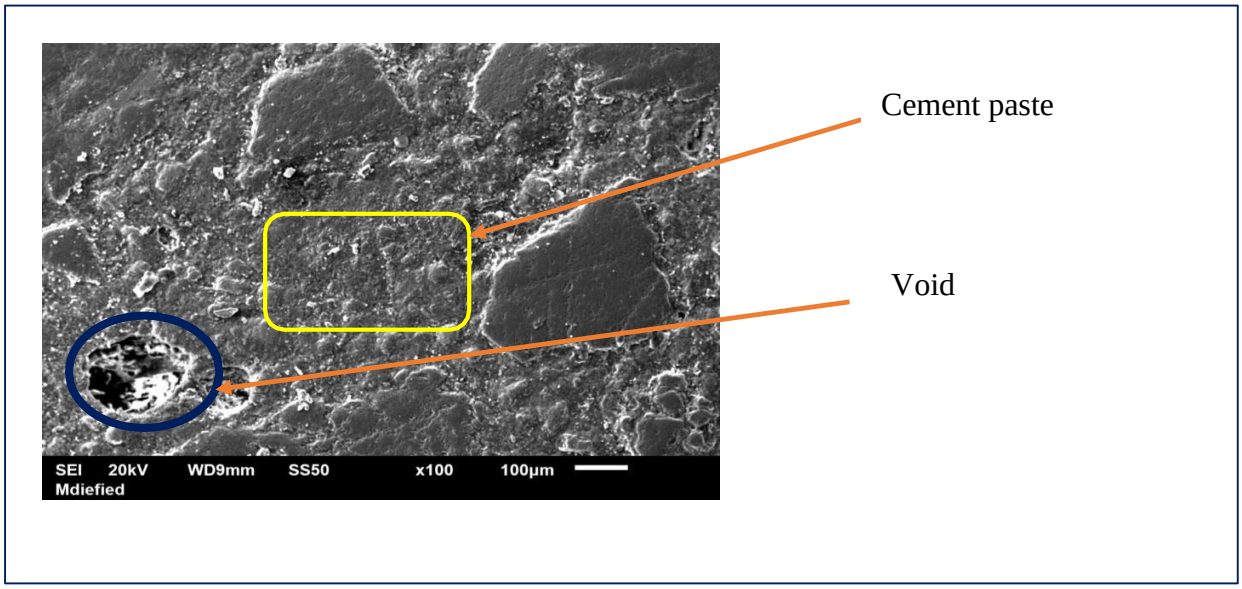

Fig 11 Microscopic view showing the formation of cement paste and voids at 5% replacement level

The dominant effect of mechanical interlocking with the surrounding cement matrix seems responsible for high strength at lower replacement levels. It is also clear that the distribution of the rubber particles is somewhat uniform at a lower level with limited voids.

In order to watch the behavior of the concrete at a higher replacement level, higher resolution SEM images were extracted. The microscopic view of concrete having 15% replacement is shown in Fig 12. This Fig. shows cement paste and its adjacent ITZ: It can be seen that the ITZ is highly porous. Identical formation of CSH gel was observed in both control and rubberized concrete.

.

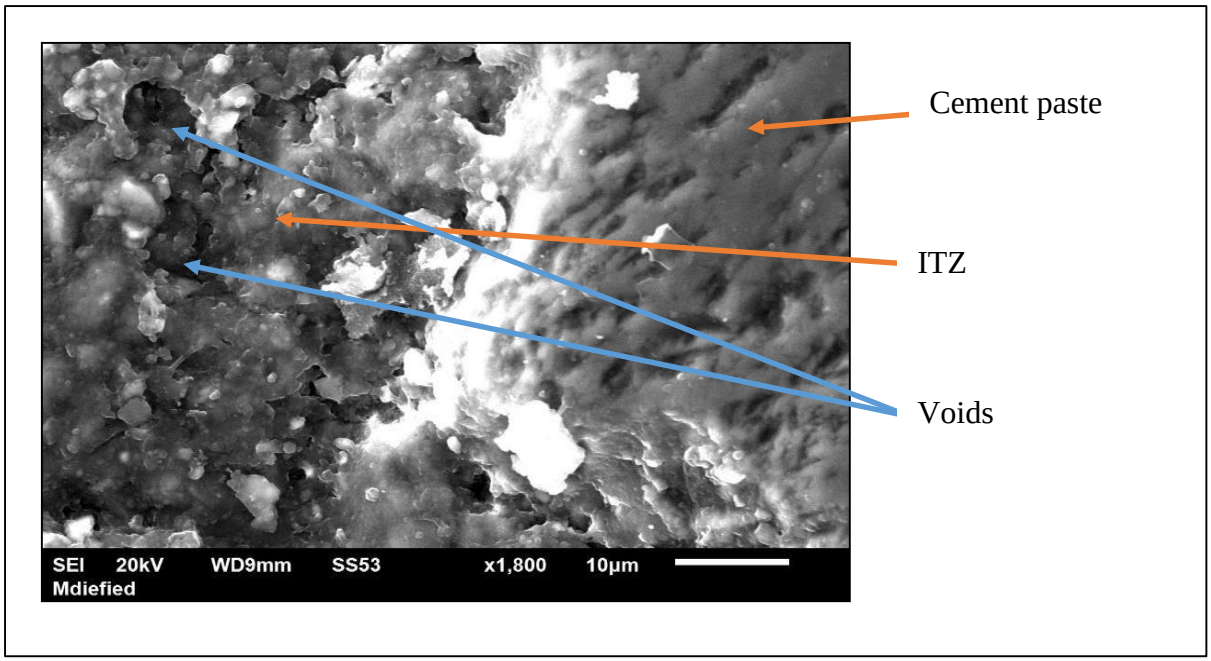

Fig 12 Microscopic view showing the formation of higher amount of voids at 15% replacement level

Fig 12 also shows that the interface bonding between the cement paste and the rubber tire is not being maintained at a higher replacement level. Due to the absence of an interfacial bonding mechanism, only mechanical interlocking can ensure stress transfer between the rubber particles and the surrounding cement paste (Fig.s 9 and 10).

Fig 13 shows a core sample of C15: The rubber particles, appeared on the surface were in the rough form. Minor traces of interface zone adhering to rubber particles were seen, which suggests a weak interfacial bonding. Some researchers have proposed NaOH-dipped crumb rubber to improve ITZ (39).

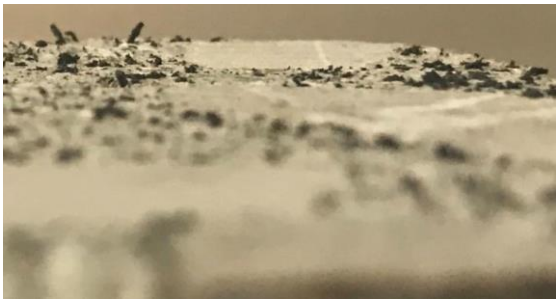

Fig 13 core sample of C15

The SEM images of Fig 10, 11 and 12 authenticate that the C-S-H morphologies of traditional concrete and rubberized concrete are the same. The addition of waste rubber tire content in normal concrete does not show any radical effect on C-S-H formation in concrete.

4. CONCLUSION

The present research intends to evaluate the concrete containing crumb rubber in different proportions, replacing sand. Based on the experimental study, the following conclusions are withdrawn:

1. The inclusion of rubber particles in place of sand ensures a true slump, which indicates cohesive concrete.

2. The partial replacement of sand by crumb rubber reduces the workability of the concrete. Replacement of 15% reduces slump beneath 25mm (ACI recommended minimum slump for ordinary concrete works).

3. Crumb rubber reduces the density of the concrete. The decrease in density is linearly related to the UPV values.

4. Crumb rubber reduces the mechanical strength of concrete. This is attributed to voids, agglomeration of rubber particles, and weaker rubber-cement paste interface. While tensile and flexural strengths decrease with rubber contents, compressive strength enhanced up to 5% replacement only.

5. Crumb rubber improves the cracking behavior of concrete and makes it more ductile.

6. SEM analysis reveals that the Interfacial transition zone of rubber concrete is weaker than that of traditional concrete: Highly porous ITZ was observed at a 15% replacement level. Air-entrainment at 15% replacement drastically reduced the workability.

7. SEM analysis manifests that the addition of rubber content does not have any notable effect on C-S-H formation in concrete.

8. Based on the results, it is concluded that ordinary containing 5% sand replaced by crumb rubber has a reasonable slump, mechanical strength, low density, and ductile behavior. This can save 5% amount of a non-renewable source (sand); secondly, the concrete can be made more sustainable by partially replacing sand by waste rubber. In many occasions, we do need a sustainable (more porous) concrete rather than a strong concrete (for example where insulation is more important and high strength is not required at all). As a matter of fact, larger replacements make concrete highly porous with low strength and extremely low workability.

ACKNOWLEDGEMENT

This research was supported by the Office of Research, Innovation, and Commercialization (ORIC), Mirpur University of Science and Technology (MUST), and GeoSciences Labs, Chak Shehzad, Islamabad. We thank our colleagues from the Civil Engineering Department, who provided due assistance during the accomplishment of this work.

Funding

This research received no external funding.

Conflicts of Interest

The authors declare no conflict of interest.

5. REFERENCES

[1]. Hilburg J. Concrete production produces eight percent of the world's carbon dioxide emissions. The Architect's Newspaper. 2019 Jan 2;

[2]. Khitab A, M. Alam, Riaz H, Rauf S. Smart Concretes: Review. Int J Adv Life Sci Technol. 2014;1(2):47–53.

[3]. SMITHERS. Global industry tire volume to reach 2.7 billion units by 2022. 2017;

[4]. Khan RBN, Khitab A. Enhancing Physical, Mechanical and Thermal Properties of Rubberized Concrete. Eng Technol Q Rev. 2020;3(1):33–45.

[5]. Khitab A. Materials of Construction. 1st ed. Lahore, Pakistan: Allied Books; 2012.

[6]. Khitab A, Anwar W. Classical Building

Materials. In: Advanced Research on Nanotechnology for Civil Engineering Applications. 2016. P. 1–27.

[7]. Munir MJ, Kazmi SMS, Wu Y-F, Patnaikuni I. A Literature Review on Alkali Silica Reactivity of Concrete. Int J Strateg Eng. 2018 Apr 12;1(2):43–62.

[8]. Kaloush K, Way GB, Zhu H. Properties of crumb rubber concrete. Transp Res Rec J Transp Res Board. 2005;1914:8–1

[9]. Ho AC, Turatsinze A, Hameed R, Vu DC. Effects of rubber aggregates from grinded used tyres on the concrete resistance to cracking. J Clean Prod. 2012 Mar;23(1):209–15.

[10]. Ghedan RH, Hamza DM. Effect Of Rubber Treatment On Compressive Strength And Thermal Conductivity Of Modified Rubberized Concrete. J Eng Dev. 2011;15(4):21–9.

[11]. Pacheco-Torgal F, Ding Y, Jalali S. Properties and durability of concrete containing polymeric wastes (tyre rubber and polyethylene terephthalate bottles): An overview. Constr Build Mater. 2012 May;30:714–24.

[12]. Thomas BS, Kumar S, Mehra P, Gupta RC, Joseph M, Csetenyi LJ. Abrasion resistance of sustainable green concrete containing waste tire rubber particles. Constr Build Mater. 2016 Oct;124:906–9.

[13]. Paine KA, Dhir RK, Moroney R, Kopasakis K. USE OF CRUMB RUBBER TO ACHIEVE FREEZE/THAW RESISTING CONCRETE. In: Challenges of Concrete Construction: Volume 6, Concrete for Extreme Conditions. Thomas Telford Publishing; 2002. P. 485–98.

[14]. Mohamad Zukri SNN, Mohd Sam AR, Ab Kadir MA, Abdul Rasid NN. MECHANICAL PROPERTIES OF CONCRETE CONTAINS WASTE TIRES EXPOSED TO HIGH TEMPERATURE. Malaysian J Civ Eng. 2017;29(2):221–31.

[15]. ASTM. ASTM C31: Standard Practice for Making and Curing Concrete Test Specimens in the Laboratory. Annu B ASTM Stand. 2013;

[16]. ASTM International. ASTM C 136 Standard Test Method for Sieve Analysis of Fine and Coarse Aggregates. Annu B ASTM Stand. 2010;04(C):1–5.

[17]. ASTM C143/C143M. Standard Test Method for Slump of Hydraulic-Cement Concrete. West Conshohocken, Pennsylvania unitedstates; 2015.

[18]. ASTM C138. Standard Test Method for Density (Unit Weight), Yield, and Air Content (Gravimetric) of Concrete. West Conshohocken, PA; 2017.

[19]. ASTM C39. ASTM C39: Standard Test Method for Compressive Strength of Cylindrical Concrete Specimens. ASTM Int. 2015;1–7.

[20]. ASTM C78/C78M. Standard Test Method for Flexural Strength of

Concrete (Using Simple Beam with Third-Point Loading). West Conshohocken, Pennsylvania unitedstates; 2018.

[21]. Brick Industry Association. Specifications for and Classification of Brick. Reston, Virginia; 2007.

[22]. ASTM C597-09. Standard Test Method for Pulse Velocity Through Concrete. 2009.

[23]. ACI 211.1-91. Standard Practice for Selecting Proportions for Normal, Heavyweight, and Mass Concrete. 1991.

[24]. Bartos P. Fresh Concrete. First. Elsevier Science; 1992.

[25]. De Brito J, Agrela F. New Trends in Eco-efficient and Recycled Concrete. Elsevier; 2019.

[26]. Marar K, Eren Ö. Effect of cement content and water/cement ratio on fresh concrete properties without admixtures. Int J Phys Sci. 2011;6(24):5752–65.

[27]. Riaz MH, Khitab A, Ahmed S. Evaluation of sustainable clay bricks incorporating Brick Kiln Dust. J Build Eng. 2019 Jul 1;24:100725.

[28]. Wu Y, Wang J-Y, Monteiro PJM, Zhang M-H. Development of ultra-lightweight cement composites with low thermal conductivity and high specific strength for energy efficient buildings. Constr Build Mater. 2015 Jul;87:100–12.

[29]. Pan Z, Li H, Liu W. Preparation and characterization of super low density foamed concrete from Portland cement and admixtures. Constr Build Mater. 2014 Dec;72:256–61.

[30]. Soni ak, mary ja. Literature review on partially replaced of crumb rubber by fine aggregate in concrete. Int j adv res basic eng sci technol. 2017;3(35):211–5.

[31]. Gerges NN, Issa CA, Fawaz SA. Rubber concrete: Mechanical and dynamical properties. Case Stud Constr Mater. 2018 Dec;9:e00184.

[32]. Chylík R, Trtík T, Fládr J, Bílý P. Mechanical properties and durability of crumb rubber concrete. IOP Conf Ser Mater Sci Eng. 2017 Sep;236:012093.

[33]. Suryakanta. 4 SPECIAL METHODS OF CONCRETE COMPACTION [Internet]. CIVILBLOG.ORG. 2014. Available from: https://civilblog.org/2014/06/09/4-special-methods-of-concrete-compaction/

[34]. Singh M. Coal bottom ash. In: Waste and Supplementary Cementitious Materials in Concrete. Elsevier; 2018. p. 3–50.

[35]. Neville AM. Properties of concrete Fourth and Final Edition. In: Perason-Prentice Hall. 2004.

[36]. Aggarwal p, aggarwal y, gupta sm. Effect of bottom ash as replacement of fine aggregates in concrete. Asian j civ eng (building housing). 2007;8(1):49–62.

[37]. Sadeghbeigi R. Fluid Catalytic Cracking Handbook. Elsevier; 2012.

[38]. Khitab A, Anwar W, Mansouri I, Tariq MK, Mehmood I. Future of civil engineering materials: A review from recent developments. Rev Adv Mater Sci. 2015;42(1).

[39]. Bušić R, Miličević I, Šipoš T, Strukar K. Recycled Rubber as an Aggregate Replacement in Self-Compacting Concrete—Literature Overview. Materials (Basel). 2018 Sep 14;11(9):1729.

E ISSN NO. 2706-9648

Pakistan Journal of Engineering

For online access, please visit:
journal.pec.org.pk

TO STUDY THE MECHANICAL PROPERTY OF CONCRETE BY INCORPORATION OF COCONUT AND GLASS FIBER

Safdar Iqbal [*1] *Sajid Ullah* [2a] *, Haris Khan* [2b], *Beenish Jehan*[2c] *, Farhan Saleh* [2d], *Ahmed Sajjad* [1a] *, Amir Sohail* [2e]

[*1] *45-Civil Engineering Battalion, Pakistan Army, Peshawar, Pakistan*
[1a] *25-Engineering Core, Engineering Battalion*
[2d] *Field Engineer , NESPAK*
[2e] *CECOS University of Science & IT, Hayatabad Peshawar*
[2b] *Department of Civil Engineering, Abasyn University Peshawar, Pakistan*
[2c] *Department of Civil Engineering, CECOS University of I.T & Emerging Sciences,*

ARTICLE INFO

Article History:
Accepted on 14 January 2022
Published on 25 July 2022

Keywords
Glass Fiber (GF), Coconut Fiber (CF), Reinforced Concrete, Cement, Fiber reinforced concrete (FRC).

ABSTRACT

The wastes are growing at exponential rate and required to be either recycled or reused in concrete, which is the second most used material in the world. The Coconut shell and Glass fibers are waste materials, which were needed to utilize in some beneficial material (like concrete) to reduce environmental facts. Under this study, coconut and glass fiber were used as reinforcement materials in concrete. The Coconut fibers were selected in three different lengths of 0.03 m, 0.06 m, and 0.09 m while glass fiber length was kept as 0.012 m. Both fibers were incorporated in concrete at the rate of 1, 3, and 6 % by the weight of cement. The results show that the workability and strength of concrete increased with longer length of fibers (Glass Fiber) and percentage addition of coconut and glass fiber. Therefore, the workability of Coconut Fiber Reinforced Concrete (CFRC) increased from 5.26 - 32.11 %, and Glass Fiber Reinforced Concrete (GFRC) increased from 4.21 – 26.26 %. Also, the strength of Coconut Fiber Reinforced Concrete (CFRC) increased from 3 - 11 % and Glass Fiber Reinforced Concrete (GFRC) increased from 4 – 10 %. The maximum workability and strength of concrete sample increased when Coconut Fiber Reinforced Concrete (CFRC) of 0.09 m length is incorporated in concrete at the rate of 6 % by weight of cement.

1. INTRODUCTION

The elimination of certain waste materials was important to safe and healthy environments special in urban areas where the population was too much as compared to rural areas. According to WWF-Pakistan, contain 250 million tons of waste materials in different cities of Pakistan [1]. Such waste materials are plastic bags, glass (Fiber), kitchen waste (Coconut fiber, vegetable fiber), construction demolition waste fabrics waste, tetra packs, etc. In these waste material coconut and glass fiber was recycled in the form of concrete to increase tensile behavior. Studying various works related to waste material in concrete by addition or replacement of cement in concrete with different percentages [2–7].

During the production of cement, a huge amount of CO_2 is released; the emission of CO_2 during cement production pollutes the environment that mainly affects human health as will causes global warming [8]. Every year in Pakistan, the demand and use of cement increase. The increased rate of cement production is shown in Fig. 1**.** The use of waste materials in concrete like coconut and glass fiber, which will reduce the amount of cement in concrete, increase the compressive and tensile behavior of concrete [9].

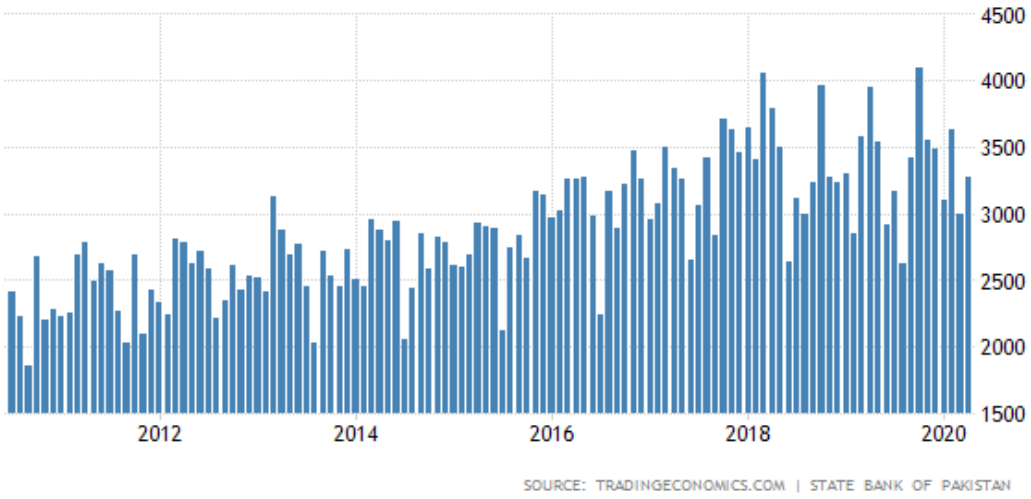

Fig. 1 - Yearly production rate of Cement in Pakistan
(Source: Trading Economics)

Concrete is an important material, and its consumption worldwide is estimated at 21–31 billion tons. Cement is the second most used substance in the world after water[10]. Concrete is a mixture of sand, gravel, and/or other combined materials bonded together with water [11].

The growing concern with the use of natural resources, driven by technological growth, increases the consumption of materials in the world. The impact of this increase causes several industrial sectors to research materials and alternatives for sustainable growth. Sustainable growth can be achieved in several ways, through the use of alternative energies, such as solar energy; water reuse, as an example its reuse as use in plantations; renewable sources, such as the use of fully biodegradable plastic bags and the use of waste, such as the use of coconut powder

reuse and recycle [12]. Composites are multiphase materials that add mechanical properties to the materials involved in this mixture, and this combination of properties has resulted in the discovery of advanced materials, with excellent mechanical properties. There are quite a few natural organic fibers in many countries around the world. Coconut is a fiber made from seeds and hair, which was obtained from the outer shell (endocarp) of the coconut shell [13–15].

The coconut fiber is 10 to 143 m long and has a diameter of 0.25 m. In addition to these parameters, high flexibility, and good strength, other plant fibers allow the use of coconut fibers to improve compound properties.

Glass fiber Concrete was popular in building materials that require creative design. GFRC was a low density and high weight strength. This makes it ideal for design panels that need to be thin but strong. The GFRC was worldwide and has a wide range of applications. Just as steel fibers were mixed with various alloys to achieve desired properties, glass fibers were made up of many chemical elements to achieve desired properties [16].

Fiberglass was the thinnest fiber, which usually contains limestone, magnesium oxide, sand, and aluminum. Glass fiber was stable, high size, easy to operate, high strength, low cost, not by the biological attack, non-chemical and has good electrical properties. Due to these properties, fiberglass was used as a reinforcing material.

The use of glass fiber allows to produce pieces of different shapes and sizes, applications in various fields of engineering and industry.

Limitations on the use of fiberglass were due to resistance to low composite fatigue, low durability module (stiffness), high abrasion, and fiber treatment, which adversely affect the operator's health [17].

Due to the strength of fiberglass concrete, it can be used for construction purposes to produce decorative panels. GFRC can be used for small and lightweight panels. This was due to its being very strong in terms of weight. Its flexibility offers a wide range of design flexibility and offers a variety of finishes, colors, textures, and patterns. A fiberglass concrete slab, weighing 20 kg / m and 10 mm thick, can reduce noise by about 30 dB. This has made it more suitable for the construction of music studios and houses where reinforced fiberglass concrete was used in home construction in the production of kitchen, industrial and commercial spaces. This was because it is sensitive to scratches and spots. Fiberglass concrete can be used for water walls as it is resistant to acid, water, lime, and salt. It, therefore, ensures that the long-term discharge was in good condition for a long time. Brick walls can be supplemented with fiberglass mesh to reinforce them, as the walls tend to withstand environmental conditions. Historical restoration has been simplified and made possible by the use of fiberglass concrete, as it can be done in the same way as copies of many constructions works[18].

As a rule, concrete has high compressive strength and low tension. Conventional concrete was characterized by a relatively low tensile strength. In structural applications, the concrete provides reinforcing bars for transmitting tensile strength after cracking of the concrete so

that it remains largely under load. In addition, the tensile strength of the concrete was much lower than that of the steel reinforcement and the cracks in the concrete before a significant load was applied to the steel [19].

There were several advantages to use fiber in concrete. One of them was a method for making concrete fibers easier than reinforcing steel beams. It was simple and easy to use, wrapping fibers can save on casting and reduce labor costs. The fibers may also be made in a thin or irregular shape; thus, the reinforcement fibers were always difficult to position when reinforcing. The only drawbacks of the fibers were the efficiency, which was lower than that of the reinforced concrete core and was not particularly effective in improving the compressive strength [20–22].

Concrete has desirable structural features such as durability, strength, and stiffness, but at the same time, there are limitations such as low removal and rapid dispersion of stress. The use of fiber as a reinforcing material is a way to reduce the limitations of this issue. For this reason, to study different literature to use the waste coconut and glass fiber as reinforced material to increase the tensile strength of concrete. In this research work, different percentages of coconut and glass fiber were added related to the weight of cement in concrete [23-24].

Fiber-reinforced concrete contains fiber with different percentages either by weight of coarse aggregates or by weight of cement

Several types of fibers were used in concrete and some examples are glass, natural and synthetic fibers [25-26]. Initially, fibers were used to prevent and control the shrinkage and drying of concrete. In addition, only one type of fiber was usually mixed with concrete. After some research, the addition of fibrous material to the concrete can also change the properties like elastic strength, elastic fatigue strength, and crack strength. In some earlier studies, more than one type of fiber has also been mixed into concrete [20–22], [27], [28]. So, therefore, in this research study, two types of fibers (Coconut and Glass fibers) were added to concrete.

2. METHODOLOGY

The physical properties of different constituents of concrete mix are described here and presented in below.

2.1 Cement

Kohat cement was used in this research work and its physical property was shown in Table 1

Table 1 – Physical Property of Cement

Properties	Values
Fineness value	1.78
Specific gravity value	3.45
Initial setting time	27.68 mins Vicat Apparatus
Final setting time	8 hrs. 30 mins Vicat Apparatus

2.2 Coarse Aggregate

The coarse aggregate used in this research work was obtained from Karak local crush plant and the physical properties were shown in Table 2.

Table 2 – Physical properties of Coarse Aggregate

Properties	Values
Size (mm)	22
Crushing Test (%)	12.4
Water Absorption (%)	0.85
Specific Gravity Value	2.58
Abrasion Test (%)	12.89
Impact Index (%)	14.68
Bulk Density (kg/m^3)	0.58

2.3 Fine Aggregate

Locally available sand in Karak was used in this research work and their physical property were shown in Table 3.

Table 3 – Physical properties of Sand

Properties	Value
Water Absorption (%)	1.368
Specific Gravity value	2.58
F.M	2.48
Rodded Unit Weight (kg)	1.589

2.4 Glass Fiber

The glass fibers were locally available everywhere in Pakistan. In this research work, we used Islamabad's available glass fiber. The market available glass fiber properties were shown in Table 4 and Fig. 2.

Table 4 - Market available glass fiber properties

Properties	Values/ Remarks
Modulus of elasticity (GPA)	75
Glass filament Dia (µ)	16
Specific gravity	2.72
Length available (mm)	12-14
Aspect ratio	860:01

Fig 2 - Locally available Glass fiber

Fig 3 - Local Available Coconut fiber in Pakistan

2.5 Coconut fiber

Coconut fiber was a waste material that is available everywhere in Pakistan like vegetable mandi, food market, etc. In this research work, the coconut fiber is collected from Islamabad's local vegetable market. The physical properties are shown in Table 5. The Fig of coconut fiber was also shown in Fig. 3.

Table 5 - Physical properties of Coconut fiber

Description	Property
Density (g/ $cm^{3)}$	0.89
Length of fiber (m)	0.03, 0.06, 0.09
Diameter of fiber (mm)	0.0044 to 0.26

After the physical property of the concrete ingredient, the concrete ratio was designed shown in Table 6.

Two concrete mixes are prepared by incorporating different amounts of fibers. In one type, coconut fibers were incorporated at the rate of 1, 3, and 6% by the weight of cement. These were designated as Control mix, CFRC-1, CFRC-3, and CFRC-6 containing 0, 1, 3, and 6 percent fibers respectively of each. These mixes were separately prepared for coconut fiber of 0.03, 0.06, and 0.09 m lengths so a total number of 10 different mixes were prepared for coconut fiber concrete shown in Table 7.

Table 6 – Concrete Mix Design

RATIO BY VOLUME	20.68 MPa		
	Cement (kg/m^3)	Fine Aggregate (kg/m^3)	Coarse Aggregate (kg/m^3)
	374	782.205	1156.8
	1.000	2.091	3.093

Table 7 - Total number of samples and addition of glass and coconut fiber

Sr. No.	Samples Description	Compressive Strength Samples			Flexure Strength Samples			Split Tensile Strength Samples			Total Samples
		7 Days	14 Day	28 Days	7 Days	14 Day	28 Days	7 Days	14 Day	28 Days	
1	Control Mix	3	3	3	3	3	3	3	3	3	28
2	CFRC 1% (CF 30 mm)	3	3	3	3	3	3	3	3	3	28
3	CFRC 3% (CF 30 mm)	3	3	3	3	3	3	3	3	3	28
4	CFRC 6% (CF 30 mm)	3	3	3	3	3	3	3	3	3	28
5	CFRC 1% (CF 60 mm)	3	3	3	3	3	3	3	3	3	28
6	CFRC 3% (CF 60 mm)	3	3	3	3	3	3	3	3	3	28
7	CFRC 6% (CF 60 mm)	3	3	3	3	3	3	3	3	3	28
8	CFRC 1% (CF 90 mm)	3	3	3	3	3	3	3	3	3	28
9	CFRC 3% (CF 90 mm)	3	3	3	3	3	3	3	3	3	28
10	CFRC 6% (CF 90 mm)	3	3	3	3	3	3	3	3	3	28
11	GFRC 1% (GF 12 mm)	3	3	3	3	3	3	3	3	3	28
12	GFRC 3% (GF 12 mm)	3	3	3	3	3	3	3	3	3	28
13	GFRC 6% (GF 12 mm)	3	3	3	3	3	3	3	3	3	28

In the second type mix design, glass fibers of 0.012 m length were incorporated in concrete at the ratio of 1, 3, and 6 % by weight of cement. These were designated as GFRC-1, GFRC-3, and GFRC-6 containing 0, 1, 3, and 6% glass fibers by weight of concrete.

Specimens were cast from all the mixes for conducting compressive strength test, flexural strength test, and split tensile strength. Compression strength tests were conducted after 7, 14, and 28 days of curing. These cylindrical specimens (0.15 x 0.30) meters were tested for each day's strength and an average value is reported. Flexural strength tests were also conducted after 7, 14, and 28 days of curing. 0.10 x 0.10 x 0.50 m dimensions of beams were tested. Three beams were tested each day and an average value of the three was reported. Split Tensile Strength tests were conducted only after 28 days. Total cylinders for this test having a size (0.15 x 0.30) meters was shown in Table 7. The Sample preparations of different mix ratios were shown in Fig. 4.

Fig. 4 Cylindrical and beam samples casting

After casting, the concrete samples were cured for 7, 14, and 28 days. The concrete samples of beams and cylinders were shown samples of beams and cylinders were shown in Fig. 5.

Fig. 5 Curing of cylindrical and beam sampl

For each strength test (Compressive, flexure, and tensile) samples were cured for the 7^{th}, 14^{th}, and 28^{th} days, this was due to check out is any change in strength concerning curing days similar to previous studies [29–31].

EXPERIMENT TEST

Different tests were performed to define the characteristic of coconut and glass fiber reinforces concrete by different percentage addition concerning cement ingredients.

In this research work, the slump test was used to find the workability of fresh concrete. The slump value of different mix ratios of coconut and Glass Fiber reinforced concrete (GFRC) was measured by slump cone, the slump procedure was shown in Fig. 6. The compressive strength of 7, 14, and 28 days of both coconut and glass fiber samples were tested in the crushing machine shown in Fig. 7. Flexural strength of 7^{th}, $14^{th,}$ and 28^{th} day's samples of both coconut and glass fiber was tested in UTM machine has shown Fig. 8. The split tensile strength of all mixes was tested in the UTM machine as shown in Fig. 9

Fig 6 Slump Test

Fig 7 Compressive test of the cylindrical sample

Fig 8 Flexural strength of the beam

Fig 9 Split tensile strength of Cylindrical Sample

4. RESULTS AND DISCUSSIONS

4.1 Slump Test

To find the workability of fresh concrete slump test was conduct for all specimens contain a different percentage of Glass and coconut fibers. The slump test result of all mix ratios was shown in Table 8 and the graphical result was shown in Fig. 10.

Table 8 - Slump values of fresh concrete

Sr. No.	Mix Type	Slump Value (mm)	Percentage Variation
1	Control Mix	48.3	-
2	CFRC 1% (CF 30 mm)	45.7	5.26%
3	CFRC 3% (CF 30 mm)	38.1	21.05%
4	CFRC 6% (CF 30 mm)	34.3	28.95%
5	CFRC 1% (CF 60 mm)	44.5	7.89%
6	CFRC 3% (CF 60 mm)	37.1	23.16%
7	CFRC 6% (CF 60 mm)	33.5	30.53%
8	CFRC 1% (CF 90 mm)	43.4	10.00%
9	CFRC 3% (CF 90 mm)	35.3	26.84%
10	CFRC 6% (CF 90 mm)	32.8	32.11%
11	GFRC 1% (GF 12 mm)	46.2	4.21%
12	GFRC 3% (GF 12 mm)	41.1	14.74%
13	GFRC 6% (GF 12 mm)	36.1	25.26%

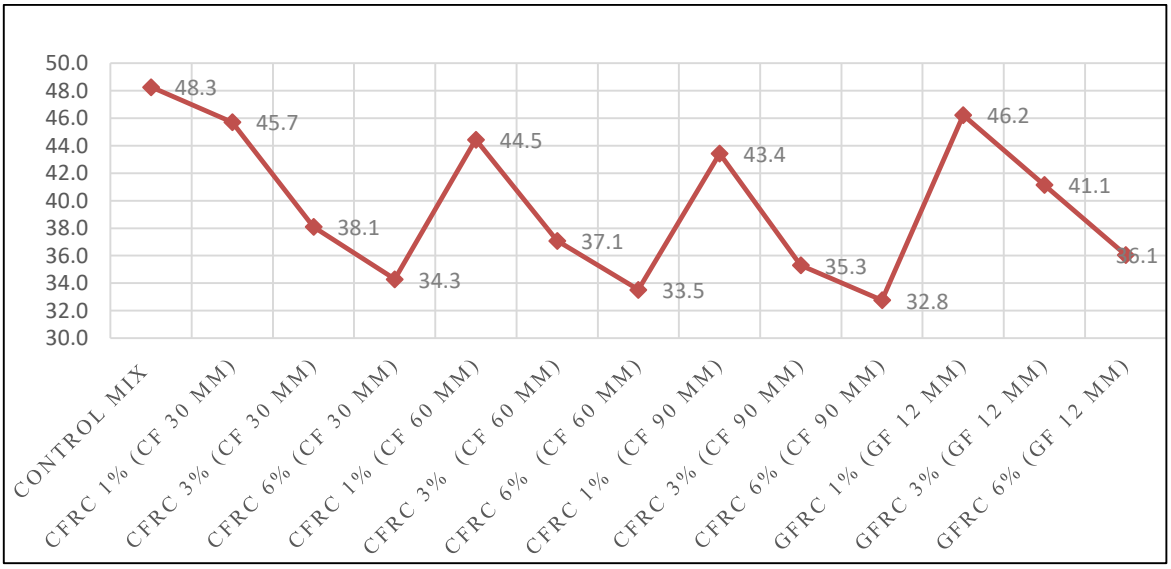

Fig 10 Graphical result of slump test

Table 8 and Fig. 10 show that the slump value of all concrete specimens decreased with the addition or incorporation of coconut fiber and glass fiber in concrete therefore, the workability of concrete decrease like the previous research work [29–31].

The decrease in workability with the addition of coconut and glass fiber of concrete was due to coconut and glass fiber absorbed water as compared to the control mix (Normal concrete).

Compare the slump values of the same percentage addition of Coconut fiber and glass fiber in concrete, show that the workability of coconut fiber concrete was greater as compared to glass fiber concrete. This was due to coconut fibers have a greater tendency to make bands with concrete constituents as compared to glass fiber. Overall comparison between mix ratios (Specimen) the slump value of the normal concrete sample was high due to there was no direct addition or incorporation of coconut or glass fiber in concrete.

The slump values of normal concrete compared with other specimen (contain coconut & glass fiber) show maximum and minimum variation from 5.26 to 32.11 %. The minimum slump is of 6 % addition of glass fiber by weight of cement which is 32.8 mm. The remaining percentage variation of different sample to the control mix was shown in Table 8.

4.2 Compressive strength

Compressive strength of 7th, 14th, and 28th day's cured samples of both coconut and glass fiber was shown in Table 9 and the graphical result was also shown in Fig. 11.

Table 9 – Compressive strength of 7th, 14^{th,} and 28th day's samples

Mix Type	7th day (MPa)	14th day (MPa)	28th day (MPa)	Percentage Variation		
				7th day (MPa)	14th day (MPa)	28th day (MPa)
Control Mix	16.31	17.35	18.69			
CFRC 1% (CF 30 mm)	16.88	17.91	19.26	3.3%	8.9%	15.3%
CFRC 3% (CF 30 mm)	17.58	18.62	19.96	7.2%	12.4%	18.3%
CFRC 6% (CF 30 mm)	18.26	19.29	20.64	10.6%	15.4%	20.9%
CFRC 1% (CF 60 mm)	17.17	18.21	19.59	5.0%	10.4%	16.7%
CFRC 3% (CF 60 mm)	17.81	18.85	20.24	8.4%	13.5%	19.4%
CFRC 6% (CF 60 mm)	18.28	19.33	20.71	10.8%	15.6%	21.2%
CFRC 1% (CF 90 mm)	17.22	18.28	19.71	5.3%	10.8%	17.2%
CFRC 3% (CF 90 mm)	17.86	18.92	20.35	8.7%	13.8%	19.8%
CFRC 6% (CF 90 mm)	18.55	19.60	21.03	12.0%	16.8%	22.4%
GFRC 1% (GF 12 mm)	17.06	18.08	19.44	4.4%	9.8%	16.1%
GFRC 3% (GF 12 mm)	17.27	18.28	19.65	5.5%	10.8%	17.0%
GFRC 6% (GF 12 mm)	18.40	19.42	20.78	11.4%	16.0%	21.5%

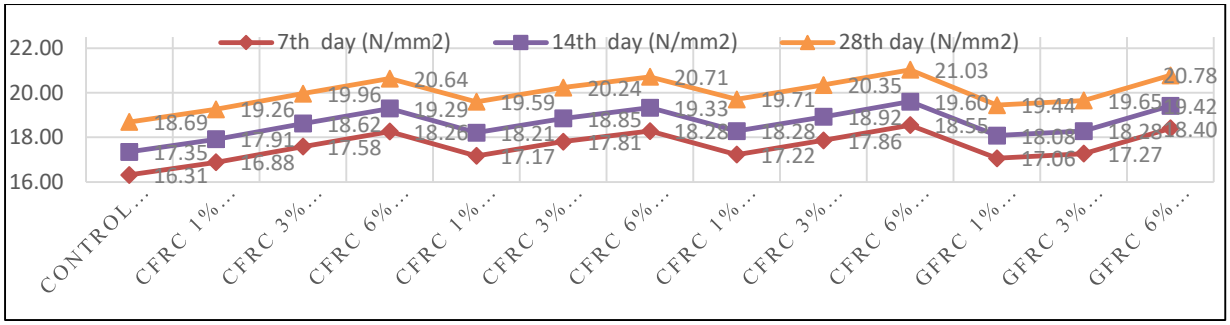

Fig. 11 Compressive strength of 7th, 14th, and 28th days

Table 9 and Fig. 11 show that the compressive strength increases with increasing the amount of coconut fiber as it will also increase with the length of coconut fiber. This was due to improve the reinforcement property of concrete [29–31]. The maximum compressive strength is 21.03 MPa of 0.09 m length coconut fiber with a 6% addition by weight cement in concrete. The increasing strength of concrete specimens by the addition of glass and coconut fiber is due to an increase in the reinforcement behavior of concrete. The glass and coconut fiber make a bond with concrete constituents and behaves like reinforcement material.

The glass fiber concrete samples have good compressive strength; the maximum compressive strength is 20.78 MPa of 6% addition of glass fiber by weight of cement. The percentage variation of different samples of coconut fiber reinforced concrete with control mix show that the compressive strength increased by weight as well as by length of fiber from 15.3% to 22.4%. Similarly, the percentage variation of glass fiber with control mix show that the strength increased from 16.1% to 21.5%.

4.3 Flexural Strength

The flexural strength result of the 7th, 14th, and 28th day samples of both coconut and glass fiber were shown in Table 10 and the graphical result was shown in Fig. 12.

Table 10 - Flexural Strength result of all samples

Mix Type	7th day (MPa)	14th day (MPa)	28th day (MPa)	Percentage Variation		
				7th day (MPa)	14th day (MPa)	28th day (MPa)
Control Mix	2.61	2.93	3.18			
CFRC 1% (CF 30 mm)	2.70	3.03	3.27	3.3%	13.8%	20.3%
CFRC 3% (CF 30 mm)	2.81	3.15	3.39	7.2%	17.0%	23.1%
CFRC 6% (CF 30 mm)	2.92	3.26	3.51	10.6%	19.9%	25.6%
CFRC 1% (CF 60 mm)	2.75	3.08	3.33	5.0%	15.2%	21.6%
CFRC 3% (CF 60 mm)	2.85	3.19	3.44	8.4%	18.1%	24.1%
CFRC 6% (CF 60 mm)	2.93	3.27	3.52	10.8%	20.1%	25.9%
CFRC 1% (CF 90 mm)	2.76	3.09	3.35	5.3%	15.5%	22.1%
CFRC 3% (CF 90 mm)	2.86	3.20	3.46	8.7%	18.4%	24.5%
CFRC 6% (CF 90 mm)	2.97	3.31	3.58	12.0%	21.2%	27.0%
GFRC 1% (GF 12 mm)	2.73	3.06	3.31	4.4%	14.6%	21.0%
GFRC 3% (GF 12 mm)	2.76	3.09	3.34	5.5%	15.5%	21.9%
GFRC 6% (GF 12 mm)	2.94	3.28	3.53	11.4%	20.5%	26.1%

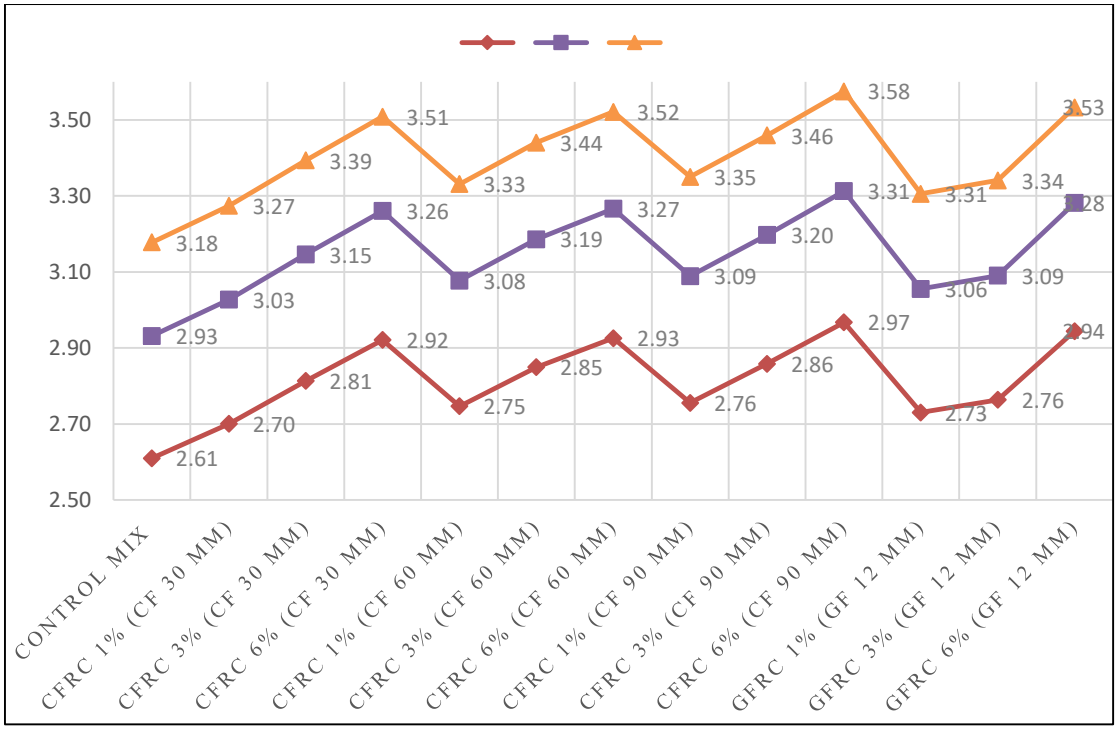

Fig 12 - Graphical result of Flexural strength

From Table 10 and Fig. 12 the compressive strength increases with an increase in the quantity of coconut and glass fiber in the concrete specimen as compared to the control mix. The maximum flexural strength is 3.58 MPa of specimen having coconut fiber (0.09 m length) of 6 % addition or incorporation of cement in concrete. Concrete is weak in tension but due to the addition of coconut and glass fiber the reinforcement behavior increases and as a result, the flexural strength will increase [7].

Similarly, the flexural strength of Glass Fiber reinforced concrete (GFRC) increases with the increase in the amount of glass fiber, the maximum flexural strength of Glass Fiber reinforced concrete (GFRC)is 3.53 MPa with 6% addition of cement in concrete.

The percentage variation of different samples of coconut fiber reinforced concrete with control mix show that the flexural strength increased by weight is will as by length of fiber from 20.3% to 27.0%. Similarly, the percentage variation of glass fiber with control mix show that the flexural strength increased from 21.9% to 26.1%.

4.4 Split Tensile Strength

Split tensile strength results of 7^{th}, 14^{th} , and 28^{th} day's samples of both coconut and glass fiber are shown in Table 11, and the graphical result shown in Fig. 13.

Table 11 - Split Tensile Strength of all samples

Mix Type	7th day (MPa)	14th day (MPa)	28th day (MPa)	Percentage Variation		
				7th day (MPa)	14th day (MPa)	28th day (MPa)
Control Mix	1.66	1.93	2.07			
CFRC 1% (CF 30 mm)	1.67	1.95	2.09	0.9%	14.9%	20.7%
CFRC 3% (CF 30 mm)	1.69	1.97	2.11	2.3%	16.0%	21.6%
CFRC 6% (CF 30 mm)	1.72	2.00	2.14	3.9%	17.2%	22.6%
CFRC 1% (CF 60 mm)	1.68	1.96	2.11	1.5%	15.7%	21.6%
CFRC 3% (CF 60 mm)	1.69	1.97	2.12	1.8%	15.9%	21.8%
CFRC 6% (CF 60 mm)	1.74	2.02	2.17	4.9%	18.2%	23.8%
CFRC 1% (CF 90 mm)	1.71	2.00	2.15	3.1%	17.2%	23.0%
CFRC 3% (CF 90 mm)	1.72	2.01	2.16	3.8%	17.7%	23.5%
CFRC 6% (CF 90 mm)	1.74	2.03	2.19	5.1%	18.6%	24.3%
GFRC 1% (GF 12 mm)	1.70	1.98	2.14	2.5%	16.6%	22.5%
GFRC 3% (GF 12 mm)	1.71	2.00	2.15	3.5%	17.4%	23.2%
GFRC 6% (GF 12 mm)	1.72	2.01	2.16	3.7%	17.5%	23.3%

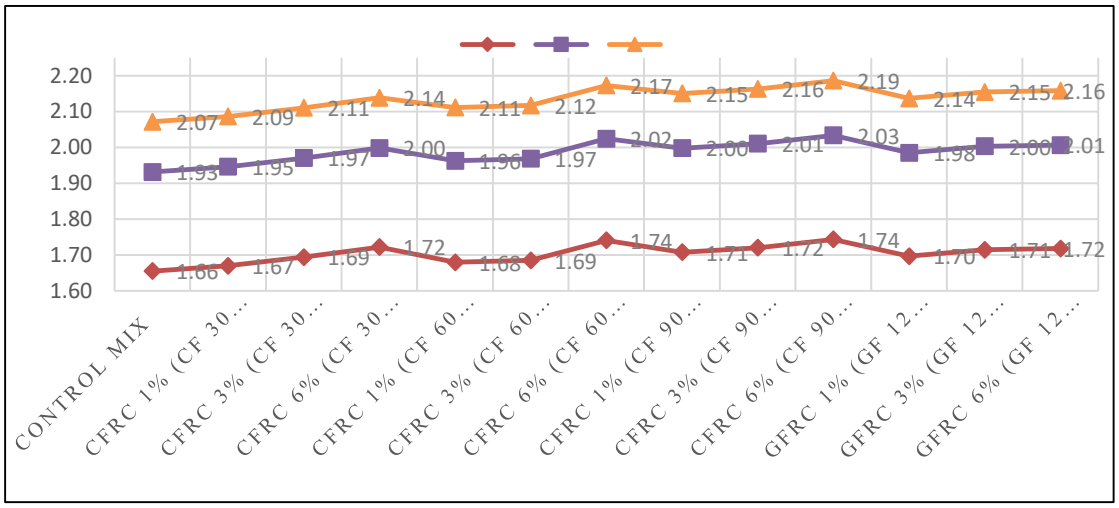

Fig. 13 Graphical result of Split Tensile Strengt

The split tensile test increases with the addition of coconut and glass fiber in concrete. The maximum split tensile strength was 2.19 MPa of coconut fiber of 0.09 m length with a 6 % addition of cement in concrete.

Similarly, the split tensile strength of Glass Fiber reinforced concrete (GFRC) increases with the increase in the amount of glass fiber, the maximum split tensile strength of Glass Fiber reinforced concrete (GFRC) was 2.16 MPa with a 6 % addition of cement in concrete.

The percentage variation of different samples of coconut fiber reinforced concrete with control mix show that the split strength increased by weight is will as by length of fiber from 20.7% to 24.3%. Similarly, the percentage variation of glass fiber with control mix show that the split strength increased from 22.5% to 23.3%.
Normal concrete is weak split tensile strength but increased due to the reinforcement property concrete with the addition of coconut and glass fiber.

6. CONCLUSION

The following conclusions are given below:

1. The Slump value decreases with increasing the amount of fiber (Coconut & Glass), as well as by increasing the length of fiber (Coconut & Glass). Therefore, the workability of concrete decreased with the addition of coconut and glass fiber. The Slump value of each sample of coconut fiber reinforced concrete with length as well as weight of fiber decreased from 5.26% to 32.11%, and similarly Glass fiber reinforced concrete decreased from 4.21% to 25.26%.

2. The compressive strength result shows that the strength increases with an increase in the quantity as well as the length of fiber (Coconut & Glass). The best compressive strength result is 6% by addition of coconut fiber of 9 cm length. The compressive strength result of the glass fiber concrete mixes ratio was also acceptable values as compared to 1% and 3% addition of coconut fiber. The compressive strength of each sample of coconut fiber reinforced concrete with length as well as weight of fiber decreased from 15.3% to 22.4% and similarly Glass fiber reinforced concrete decreased from 16.1% to 21.5%.

3. Similarly, the flexural strength is increasing with increases of the quantity as well as the length of fiber (Coconut & Glass). The greater flexural strength is 433.07 psi at 6% addition of coconut fiber of 9 cm length. The second highest flexural strength is 424.4 psi at 6% addition of glass fiber of 12 m length. The flexural strength of each sample of coconut fiber reinforced concrete with length as weight of fiber decreased from 20.3% to 27.0%, and similarly Glass fiber reinforced concrete decreased from 21.0% to 26.1%.

4. The split tensile strength is also increased with an increase in the quantity and length of fiber (Coconut & Glass). The greater split tensile strength is 317.06 psi of 6 % addition of coconut fiber of 9 cm length. The second highest split tensile is 312.99 psi of 6% addition of glass fiber of 12 m length. The flexural strength of each sample of coconut fiber reinforced concrete with length as well as weight of fiber decreased from 20.7% to 24.3% and similarly Glass fiber reinforced concrete decreased from 22.2% to 23.3%.

5. Overall, the strength parameters of concrete increased with the addition of coconut and glass fiber quantity as well as length of coconut fiber.

5 RECOMMENDATIONS

The following recommendation was given in this research work.

1. The highest compressive strength is achieved on a 6% addition of cement by coconut fiber as well as glass fiber.
2. Similarly, the highest flexure and split tensile strength is achieved on a 6% addition of cement by coconut fiber as well glass as fiber.

6. SUGGESTION FOR FUTURE WORK

Following are the future recommendations:

i. To check further percent increase of coconut fiber as well as glass fiber in concrete up to 12%.
ii. To check the combined effect of coconut and glass fiber in concrete with different mix ratios.
iii. To check CFRC and GFRC against acid and sulfate attack.

ACKNOWLEDGMENTS

The research described in this paper has no funding.

REFERENCES

[1] "Plastic Pollution," pp. 115–147, 2020, doi: 10.1142/9781786347435_0005.

[2] M. S. Khan, M. Sohail, N. S. Khattak, and M. Sayed, "Industrial ceramic waste in Pakistan, valuable material for possible applications," *J. Clean. Prod.*, vol. 139, pp. 1520–1528, 2016, doi: 10.1016/j.jclepro.2016.08.131.

[3] Saeed MA, Irshad A, H. Sattar, A. G. E, Phylaktou H N, and & Gibbs, "Agricultural Waste Biomass Energy Potential in Pakistan," *Int. Bioenergy Exhib. Asian Bioenergy Conf.*, no. February 2020, pp. 21–23, 2015, [Online]. Available: http://eprints.whiterose.ac.uk/98565/%0Ahttp://eprints.whiterose.ac.uk/98565/.

[4] H. Arshad, M. Qasim, M. J. Thaheem, and H. F. Gabriel, "Quantification of material wastage in construction industry of Pakistan: An analytical relationship between building types and waste generation," *J. Constr. Dev. Ctries.*, vol. 22, no. 2, pp. 19–34, 2017, doi: 10.21315/jcdc2017.22.2.2.

[5] P. Ishtiaq, S. A. Khan, and M. U. Haq, "A multi-criteria decision-making approach to rank supplier selection criteria for hospital waste management: A case from Pakistan," *Waste Manag. Res.*, vol. 36, no. 4, pp. 386–394, 2018, doi: 10.1177/0734242X18755894.

[6] M. Khan and M. Ali, "Effect of super plasticizer on the properties of medium strength concrete prepared with coconut fiber," *Constr. Build. Mater.*, vol. 182, pp. 703–715, 2018, doi: 10.1016/j.conbuildmat.2018.06.150.

[7] W. Ahmad *et al.*, "Effect of coconut fiber length and content on properties of high strength concrete," *Materials (Basel).*, vol. 13, no. 5, 2020, doi: 10.3390/ma13051075.

[8] A. Bosoaga, O. Masek, and J. E. Oakey, "CO2 Capture Technologies for Cement Industry," *Energy Procedia*, vol. 1, no. 1, pp. 133–140, 2009, doi: 10.1016/j.egypro.2009.01.020.

[9] B. Lin and M. Y. Raza, "Analysis of energy related CO 2 emissions in Pakistan," *J. Clean. Prod.*, vol. 219, pp. 981–993, 2019, doi: 10.1016/j.jclepro.2019.02.112.

[10] D. S. Vijayan, Dineshkumar, S. Arvindan, and T. S. Janarthanan, "Evaluation of ferrock: A greener substitute to cement," *Mater. Today Proc.*, vol. 22, pp. 781–787, 2020, doi: 10.1016/j.matpr.2019.10.147.

[11] A. J. Field, “Ideology, economic policy, and economic history: Cohen and DeLong’s Concrete Economics,” *J. Econ. Lit.*, vol. 55, no. 4, pp. 1526–1555, 2017, doi: 10.1257/jel.20161442.

[12] A. Gupta, N. Gupta, A. Shukla, R. Goyal, and S. Kumar, “Utilization of recycled aggregate, plastic, glass waste and coconut shells in concrete - A review,” *IOP Conf. Ser. Mater. Sci. Eng.*, vol. 804, no. 1, 2020, doi: 10.1088/1757-899X/804/1/012034.

[13] K. Gunasekaran, R. Annadurai, and P. S. Kumar, “A study on some durability properties of coconut shell aggregate concrete,” *Mater. Struct. Constr.*, vol. 48, no. 5, pp. 1253–1264, 2015, doi: 10.1617/s11527-013-0230-2.

[14] T. Liu, S. Hou, X. Nguyen, and X. Han, “Energy absorption characteristics of sandwich structures with composite sheets and bio coconut core,” *Compos. Part B Eng.*, vol. 114, pp. 328–338, 2017, doi: 10.1016/j.compositesb.2017.01.035.

[15] D. Vinay Kumar, N. Mohan, and A. K. Bongale, “Fabrication and tribological investigation of Coconut coir/Banana fiber/Glass fiber reinforced hybrid polymer matrix composites- A Taguchi’s approach,” *Mater. Res. Express*, vol. 6, no. 10, 2019, doi: 10.1088/2053-1591/ab3d4a.

[16] K. I. M. Ibrahim, “Mechanical Properties of Glass Fiber Reinforced Concrete (GFRC),” *IOSR J. Mech. Civ. Eng.*, vol. 13, no. 04, pp. 47–50, 2016, doi: 10.9790/1684-1304054750.

[17] A. B. Kizilkanat, N. Kabay, V. Akyüncü, S. Chowdhury, and A. H. Akça, “Mechanical properties and fracture behavior of basalt and glass fiber reinforced concrete: An experimental study,” *Constr. Build. Mater.*, vol. 100, pp. 218–224, 2015, doi: 10.1016/j.conbuildmat.2015.10.006.

[18] H. Kasagani and C. B. K. Rao, “Effect of graded fibers on stress strain behaviour of Glass Fiber Reinforced Concrete in tension,” *Constr. Build. Mater.*, vol. 183, pp. 592–604, 2018, doi: 10.1016/j.conbuildmat.2018.06.193.

[19] A. A. S. Correia, P. J. Venda Oliveira, and D. G. Custódio, “Effect of polypropylene fibres on the compressive and tensile strength of a soft soil, artificially stabilised with binders,” *Geotext. Geomembranes*, vol. 43, no. 2, pp. 97–106, 2015, doi: 10.1016/j.geotexmem.2014.11.008.

[20] J. Wei and C. Meyer, “Improving degradation resistance of sisal fiber in concrete through fiber surface treatment,” *Appl. Surf. Sci.*, vol. 289, pp. 511–523, 2014, doi: 10.1016/j.apsusc.2013.11.024.

[21] G. M. Sadiqul Islam and S. Das Gupta, “Evaluating plastic shrinkage and permeability of polypropylene fiber reinforced concrete,” *Int. J. Sustain. Built Environ.*, vol. 5, no. 2, pp. 345–354, 2016, doi: 10.1016/j.ijsbe.2016.05.007.

[22] Ls. Raju and D. Mathur, “International Journal of Emerging Technology and Advanced Engineering Polypropylene Fiber Reinforced Concrete-A Review,” *Certif. J.*, vol. 9001, 2008, [Online]. Available: www.ijetae.com.

[23] N. Karimi and D. Mostofinejad, “Bacillus subtilis bacteria used in fiber reinforced concrete and their effects on concrete penetrability,” *Constr. Build. Mater.*, vol. 230, 2020, doi: 10.1016/j.conbuildmat.2019.117051.

[24] D. Y. Yoo and N. Banthia, "Mechanical and structural behaviors of ultra-high-performance fiber-reinforced concrete subjected to impact and blast," *Constr. Build. Mater.*, vol. 149, pp. 416–431, 2017, doi: 10.1016/j.conbuildmat.2017.05.136.

[25] S. M. Hejazi, M. Sheikhzadeh, S. M. Abtahi, and A. Zadhoush, "A simple review of soil reinforcement by using natural and synthetic fibers," *Constr. Build. Mater.*, vol. 30, pp. 100–116, 2012, doi: 10.1016/j.conbuildmat.2011.11.045.

[26] N. Banthia, V. Bindiganavile, J. Jones, and J. Novak, "Fiber-reinforced concrete in precast concrete applications: Research leads to innovative products," *PCI J.*, vol. 57, no. 3, pp. 33–46, 2012, doi: 10.15554/pcij.06012012.33.46.

[27] T. Ayub, N. Shafiq, and M. F. Nuruddin, "Mechanical properties of high-performance concrete reinforced with basalt fibers," *Procedia Eng.*, vol. 77, pp. 131–139, 2014, doi: 10.1016/j.proeng.2014.07.029.

[28] V. Afroughsabet, L. Biolzi, and T. Ozbakkaloglu, "High-performance fiber-reinforced concrete: a review," *J. Mater. Sci.*, vol. 51, no. 14, pp. 6517–6551, 2016, doi: 10.1007/s10853-016-9917-4.

[29] D. Neeraja, A. I. Wani, Z. Kamili, and K. Agarwal, "Study on strength characteristics of concrete using M-Sand and coconut fibers," *IOP Conf. Ser. Mater. Sci. Eng.*, vol. 263, no. 3, 2017, doi: 10.1088/1757-899X/263/3/032014.

[30] A. Garg and P. K. Sharma, "Mechanical properties of glass fiber reinforced concrete with recycled aggregates," *J. Appl. Sci. Eng.*, vol. 24, no. 6, pp. 1033–1039, 2021, doi: 10.6180/jase.202112_24(6).0018

[31] R. Lala and G. Batham, "Glass Fibre High Strength Concrete , an Alternate to Conventional Concrete," pp. 2–7.

E ISSN NO. 2706-9648

Pakistan Journal of Engineering

For online access, please visit:
journal.pec.org.pk

IMPROVED GREY WOLF OPTIMIZATION IMPLEMENTED ON ECONOMIC LOAD DISPATCH PROBLEM.

Ali Hassan[*1], *Muhammad Awais Ali*[2], *Ashfaq Ahmed*[3]

[*1] *Ali Hassan, Instructor Electrical, Department of Electrical Engineering, TEVTA Punjab*
[2] *Muhammad Awais Ali, Instructor Electrical, Department of Electrical Engineering, TEVTA Punjab*
[3] *Dr. Ashfaq Ahmed, Assistant Professor, Department of Electrical Engineering, MUST AJK*

ARTICLE INFO

Article History:
Accepted on 29 March 2022
Published on 25 July 2022

Keywords
Economic Load Dispatch,
Fuel Cost Function,
Valve Point Loading Effect, Prohibited Zones.

ABSTRACT

The economic load dispatch (ELD) is an important power system in operational planning. Economic load dispatch is practically a critical problem in power system operation because of its non-linear and complex behavior in nature. Initially mathematically/calculus techniques have been used for solving ELD problems but have a lot of convergence issues. Later on, Artificial Intelligence Techniques have been developed, one of which is Grey Wolf Optimization (GWO) applied on ELD problem and suffers from convergence issue and do not search globally. To overcome this issue, the proposed improved grey wolf optimization (IGWO) is integrated with mutation and crossover operations to enhance the performance of GWO to resolve ELD problem. IGWO with its robustness is applied on three ELD problems 6, 13 and 15 thermal units test system and compared with recent techniques. This comparison proves the superiority of IG.

1. INTRODUCTION

The principle on which business can flourish is to have maximum output at lowest cost to maintain the quality standards. Power system planning and operation includes the study of different problems like Economic dispatch, stability of system, system protection, load management, power factor controlling and unit commitment. Economic Load Dispatch (ELD) [1] is termed as the useful solution to the maximum output of set electric generators at lowest possible operating cost by meeting the demand load, ensuring the transmission and other constraints.

Initial practices of economic dispatch in power system are to supply power from most resourceful plant to meet the load. The scheme was set that to put variable load on best efficient power plant untill it reaches

its maximum limit then the remaining load is put on the next most effective power plant. In this way, the load is met but this practice is not cost effective [2]. The cost per unit getting from this generation scheme is high. Looking the need of new operating scheme rises to counter the fuel cost at effective use of plants satisfying the load demand [3]. To solve the ELD issue, alot of efforts have been put using various optimization techniques. The top most techniques which have been used in the past to solve the ELD are conventional mathematical techniques. These methods consist of lambda iteration [4], Quadratic programming [5], gradient search [6] and linear programming [7]. These techniques for global optimization solution require piecewise linear and monotonically increasing fuel costs but are not valid for those generators which have non-monotonically increasing fuel costs. Valve point loading effect (VPL) and non-permitted operating zones (POZ) make objective function of economic dispatch discontinuous and non-convex and stuck at local minima.

Dynamic programming is an important optimization technique. It can resolve non-linear and non-convex ED problems, but it suffers from dimensionality problem, large computational effort is required to solve ELD issues [8-9]. To overcome the said limitations, Artificial Intelligence (AI) has been developed which is also known as meta-heuristic optimization algorithm used for solving global optimization problem in recent years [9]. These are categorized into single solution-based techniques and population-based techniques. These categories have their own dimensions and importance for solving global optimization problems. Artificial approaches has been developed like Genetic Algorithm(GA) [3], Simulated Annealing (SA) [10], Tabu Search(TS) [11], Particle Swarm Optimization (PSO) [12] ,Differential Evolution (DE) [3], krill herd algorithm (KHA) [13], Ant and Bee colony optimization(ANC)[14], Chaotic Bat Algorithm (CBA), Kinetic Gas Molecular optimization (KGMO) [15], Algorithm integrated with arithmetic crossover operator (ACHS) [16], Backtracking Search Algorithm (BSA) [17], Fuzzy and self-adaptive particle swarm optimization (FAPSO) [18], Grey wolf optimization (GWO) [19], and Improved Grey Wolf Optimization for ELD [22] .

GWO gives the best result in comparison to other swarm intelligence techniques but itself suffers from convergence issue, took more iteration to reach best value and don't search globally and stuck at local best value. These issues are resolved in proposed improved grey wolf optimization (IGWO) algorithm and furthermore better results are achieved as compared to GWO, IGWO and other swarm intelligence techniques.

1.1 Problem Articulation

Economic load Dispatch allocates the real power to fulfil the following constraints while minimizing the total fuel/running cost of thermal power plant stations.

- To meet the total demanded load
- To meet the max and min generation limits of each Generators
- Prohibited zones must be satisfied

The target is to cutdown the fuel cost of thermal generation. It is the total fuel cost to the given load demand. Mathematically fuel cost [13, 19] is given by:

Minimize: $F_t=\sum_{i=1}^{n} Fi(Pgi)$ (1)

Where F_t expresses the fuel cost of generation, F_i is the fuel cost of ith generator and P_{gi} is the real power generation of generators. There are two types of ELD problems which need to be considered are linear and nonlinear. The linear characteristics are represented by quadratic curve. The linear/ convex [4-13] behaviour of thermal units is modelled as:

$$F_i = (Pg_i) = a_i + b_i Pg_i + c_i Pg_i^2 . \quad (2)$$

P_{gi} is the active power of generator.

a, b and d are the cost coefficients of thermal generator.

In practical, thermal power plant have multiple valve operations. The fuel controlling by the valves significantly change the input/output characteristics of thermal units. This effect is considered by adding a sinusoidal term in the objective function. This results into non-linearity in the aspects of thermal units. The non-convex behavior [13] of thermal units is modelled as;

$$F_i(Pg_i) = a_i + b_i Pg_i + c_i Pg_i^2 + \left| e_i \times \mathrm{Sin}(f_i \times (P_{i,\min} - P_i)) \right| . \quad (3)$$

a, b and d are the cost coefficients of thermal generators, whereas e and f are cost coefficients reflecting valve point effect.

ELD is a multi-constrained optimization problem. This contains voltage constraint, generation capacity limits, power balance constraint, transmission losses and boundaries of operating zones. Above mentioned constraints must be satisfied in the ELD.

1.1.1 Voltage Constraint

Voltage must have same value and phase angle at various points. These values of both magnitude and phase angle must be within the specified range [18].

$$V_{i,\min} \le V_i \le V_{i,\max} . \quad (4)$$

$V_{(i,min)}$ and $V_{(i,max)}$ min and max limits of voltage of ith generator.

1.1.2 Power Balance Constraint

If the ordered load and losses are sum up this will be equal to total generation [4,18][19].

$$\sum_{i=1}^{n} P_i = P_D + P_{Loss} . \quad (5)$$

1.1.3 Generation Constraint

The output of a generator would be such that it follows the limits either it is real or reactive power [13,18].

$$P_{i,min} \le P_i \le P_{i,max} . \quad (6)$$

$P_{(i,min)}$ and $P_{(i,max)}$are min and max limits of voltage of ith generator.

1.1.4 Transmission Loss Constraints

Distance between load centers and power houses are very large. So, there are significant transmission losses and cannot be neglected. B coefficient method is used for considering transmission loss. These losses [18] can be modelled as:

$$P_{Loss} + \sum_{i=1}^{n}\sum_{j=1}^{n} P_i B_{ij} P_j + \sum_{i=1}^{n} B_{oi} P_i + B_{oo} . \quad (7)$$

B_{oo} = Constant

B_{oi} = Vector of same dimension as P_i

B_{ij} = Loss coefficient matrix

1.1.5 Prohibited Zones

Each generator has some boundaries where its operation is avoided. These boundaries are known as prohibited operating zones (POZ). The reason lies in the fact that these generation zones produce vibrations in bearings of shaft. So, due to this, shaft may damage. In order to avoid that damage these generation zones are avoided.

2 GREY WOLF OPTIMIZATION

Swarm Intelligence (SI) is one of the major classes in the class of AI techniques. SI techniques followed the living, hunting behaviour of school of fishes, flocking of birds, colonies of ants etc. Various SI algorithms have been developed for resolving optimization problems. Mirjalili et.al in 2014 produced this new Grey Wolf Optimization (GWO) [20]. GWO has been implemented on ED problem by Pradhan et al. in 2016 [19].

2.1 Social Hierarchy

Grey wolves love to live in herd. They form group to hunt. There are four types of wolves in a pack namely alpha, beta, delta and omega wolves. The grey wolves are smart worker, and they follow a leadership hierarchy.

Alpha is the commander of the grey wolves' pack. Alpha is responsible for every type of decision making in the pack. They have best information about the prey. Therefore, alpha is considered as best wolf in the pack. All other wolves follow the decisions made by alpha wolves. The second in command is beta wolves. They support alpha in taking decision. When alpha passed away then beta becomes the best candidate for leadership. In hierarchy the third group is the delta wolves. The delta wolf obeys alpha and beta. Delta wolves provide security to the grey wolves' pack. In the last omega comes. Omega wolves are the ordinary wolves. These wolves obey all other wolves in the group. These wolves do not involve in decision making process and just there to help above said hierarchy. These omega wolves can eat when all other wolves finish eating.

2.2 Mathematical Modeling Of Improved Grey Wolf Optimization

GWO mathematical modelling is for finding of optimal prey position when applied on ELD, led by alpha, and followed by other groups. The best prey location represents the optimal generation scheduling which results into minimum fuel cost. The wolf with the less fuel cost becomes alpha. The GWO technique provided good results, but better results can be achieved. Due to lack of global searching GWO suffers from stagnation problem, took more iterations to reach best result. For best results we must overcome this issue. We have operators like mutation which has greater global searching ability. In our research mutation and cross over operation is integrated into GWO to increase global searching ability and to avoid premature convergence of algorithm to achieve better output. In this research DE based mutation and crossover operations are being considered and topology would be named as "Solution to Economic Dispatch Problem using Improved Grey Wolf Optimization (IGWO)". The hunting behaviour of grey wolves is modelled in three steps:

- Searching operation (Exploration of search space)
- Encircling operation
- Hunting the prey
- Attacking (Exploitation of search space)
- Mutation
- Crossover

2.3 Searching Operation

In first half of iterations, omega group deviates from the target estimated by other groups. For modelling this behaviour, used vector *A*. It is given by [4,19]

$$A = 2a \times r1 - a . \quad (8)$$

$$B = 2 \times r2 . \quad (9)$$

r1 and r2 represents the random vectors and a decrease from 2 to 0.

When *A* mode is greater the 1, then wolves divert from the target in search of best prey. For the best solution, this is basically the exploration of search space.

2.4 Encircling

The alpha, beta and delta wolves are considered as three best wolves based on their information about prey. The omegas update their positions based on the positions of alpha, beta and delta wolves. Encircling operation [4,19] is represented by *D;*

$$D = \left| C \times X_p - X(t) \right| . \quad (10)$$

Where X_p is the position vector of prey, X(t) is the position vector of grey wolf.

Obstacles in nature are represented by vector C and No. of iterations represented by t. Since the position vector of prey is unknown and we know that alpha, beta and delta have best information about the target, so we use the position vectors [4] of these wolves. In the first iteration Dα is the best global solution.

$$D\alpha = \left| C1 \times X_\alpha - X^i(t) \right|$$
$$D\beta = \left| C2 \times X_\beta - X^i(t) \right| \quad (11)$$
$$D\delta = \left| C3 \times X_\delta - X^i(t) \right|$$

2.5 Hunting Operation

After encircling operation alpha wolves initiate hunting by computing X*i*(t+1). The position of omega wolves are updated relative to position of alpha, beta, and delta wolves [19].

$$X1 = X_\alpha - (A1 \times D_\alpha)$$
$$X2 = X_\beta - (A2 \times D_\beta) . \quad (12)$$
$$X3 = X_\delta - (A3 \times D_\delta)$$

The new population of grey wolves based on positions of alpha, beta and delta wolves is given by;

$$X_i(t+1) = \frac{(X_1 + X_2 + X_3)}{3} . \quad (13)$$

Where *i* = 1, 2....

2.6 Attacking

For last half iterations the grey wolves jump over and attack on prey is launched. When A mode is less than 1 then grey wolves attack the prey.

2.7 Mutation

Apply the mutation operation [13]

$$P^i = P^{gbest} + F(P_a - P^b) . \quad (14)$$

Where $i = 1,2,3,\ldots, Nw, i \neq gbest, a \neq b \neq i \neq gbest$.

The mutation scaling factor is represented by '*F*'. Its value ranges from 0.4 to 1. This factor controls the global searching ability of optimization process.

2.8 Crossover

Apply the crossover operation. Uniform crossover will be used. After this operation *ith* component of *ith* wolf will be given by [13]

$$P_j^i = \begin{cases} P_j^r \ldots\ldots\ldots\ldots\ldots if rand < C_r \\ P_j^r \ldots\ldots\ldots\ldots\ldots else \end{cases} . \quad (15)$$

Where $j = 1,2,\ldots D, i = 1,2\ldots Nw$, *Cr* is the crossover probability

In proposed IGWO crossover probability is

not a constant rather it depends upon the relative fitness of an individual in the population and it is defined as:

Cr = 0.2 * relative Fitness. (16)

Relative Fitness = $F^{i} - F^{best} \big/ F^{worst} - F^{best}$. (17)

These equations show that for best wolf relative fitness will be zero hence crossover probability will also be zero. For worst wolf in the population relative fitness will be 2 so crossover probability will also be 2. So, we conclude that crossover probability ranges from 0 to 2.

2.9 Flow Chart

The flow chart Fig.1. shows the mathematical modelling working mechanism in MATLAB stepwise.

Step 1: Real power generation of all the alternators is initialized randomly including their limits and constraints.

Step 2: Fitness of every solution of current position is evaluated using equation 1 to 3. Fitness will represent the how far is wolf from its prey.

Step 3: Alpha, beta and gamma wolves are categorized based on fitness value.

Step 4: Using the equations from 8 to 13 the positions of wolves are updated. The position of each agent will represent the real power output of ELD problem.

Step 5: Apply mutation and cross over on the updated positions to change the genetics of the wolves so, that they will update their positions once again and nearer to the best solution.

Step 6: Check the limits and constraints mentioned either they are justified or not. If not, then program will ensure requirements should meet.

Step7: Program will go to step 2 until max iterations reached.

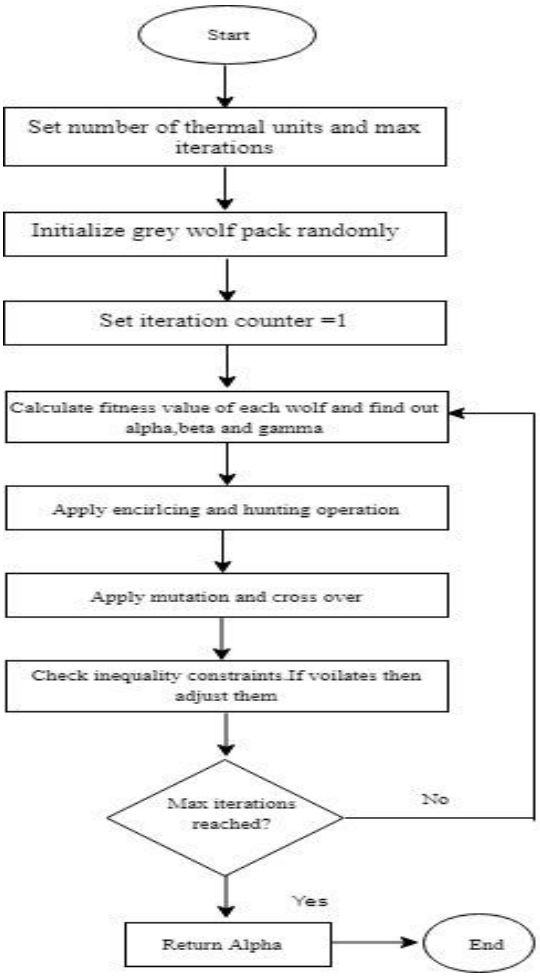

Fig 1 – Flow chart of IGWO algorithm.

3 COMPARISION OF RESULTS AND DISCUSSION

The proposed Improved grey wolf optimization is implemented on 6, 13 and 15-units standard test cases. Linear, nonlinear, transmission losses, valve point effect and prohibited zones are also deal with. B coefficient method is used for evaluating transmission losses.

3.1 Test Case 01

This contains six No units, linear test case 1263MW are considered. POZ's and transmission losses are count for this test

case and the data is as per IEEE standard.

Table 1. Shows the statistical data of the six generators at 1263MW. It shows the generation of each generator with the limits $Pg(\min)$ and $Pg(\max)$ to compare.

The number of wolves for this case taken is 30 and maximum iterations are 300. The last three rows show the demanded load of the consumer, total generation of the powerhouse, total losses and last but not the least the cost 15377($/hr) of the generator which is the target.

Fig.2. Gives the convergence characteristics for six units test system. It shows that the suggested technique converges to the most favourable point before maximum number of iterations reached.

Table 2. Shows the achievement of proposed IGWO in getting better results as compared with other techniques. Three columns are made which contain min cost, average cost and max cost. The best cost ranges from 15450.85 to 15442 ($/hr) and the IGWO gives 15377 ($/hr) cost. From this it's evident that proposed IGWO gives

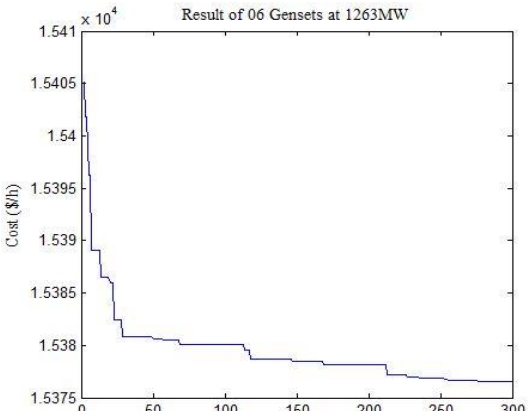

Fig 2– Rate of achieving optimal solution of 06 units at 1263MW load.

the best value compared to its other techniques. Furthermore, 65 ($/hr) savings leads to large scale benefit when we look it into month and year.

Table 1 – Results for 06 units with load = 1263MW.

Generator#	Pg.(min)MW	Pg.(max)MW	Output MW
1	100	444.4810	444.4810
2	50	200	171.1699
3	80	300	261.6562
4	50	150	150.0000
5	50	200	162.9039
6	50	120	85.0000
Demanded Load			1263 MW
Total Generation			1275.2 MW
Total Losses			12.2111 MW
Total Cost ($/hr)			15377

Table 2 – Comparison of 06 units with other techniques.

Techniques	Min Cost($/hr)	Average Cost ($/hr)	Max Cost($/hr)
PSO [21]	15450.84	-	15492
NAPSO [18]	15443.76	15443.76	15443.765
DE [3]	15449.766	15449.777	15449.874
KHA-4 [13]	15443.0752	15443.1863	15443.3265
GWO [19]	15443	15444	15445
IGWO[22]	15442	15442.6	15445
Proposed IGWO	15377	15381.2	15390.2

3.2 Test case 02

Proposed IGWO is tested on 13 units standard test system. The load demands are 1800 MW and 2520MW in the case as per IEEE standard. The number of wolves for this case taken is 30 and maximum iterations are 1000.The valve point loading effect is also being considered along with the losses.

3.2.1 Case A

Proposed IGWO is tested on 13 units standard test case with load 1800 MW. The VPL effect is also being considered. Table 3. Shows the min and max limits of the generator and the generation against each generator. The total load which is demanded 1800MW is fulfilled and the losses are 20MW overall at the cost of 17490 ($/hr.). Losses are considered using B coefficient method.

Table 3 – Results for 13 units with load = 1800MW.

Generator #	Pg.(min) MW	Pg.(max) MW	Output MW	Generator #	Pg.(min) MW	Pg.(max) MW	Output MW
1	0	680	628.3923	8	60	180	60.0000
2	0	360	81.5241	9	60	180	60.0000
3	0	360	360.0000	10	40	120	40.0000
4	60	180	60.0000	11	40	120	120.0000
5	60	180	60.0000	12	55	120	55.1166
6	60	180	180.0000	13	55	120	55.0473
7	60	180	60.0000				
Demanded Load							1800 MW
Total Generation							1820.1 MW
Total Losses							20.0802 MW
Total Cost ($/hr)							17490

Fig.3. gives the convergence characteristics for thirteen units test. It shows that the suggested algorithm converges to the best point smoothly, too fast and before last iteration reached.

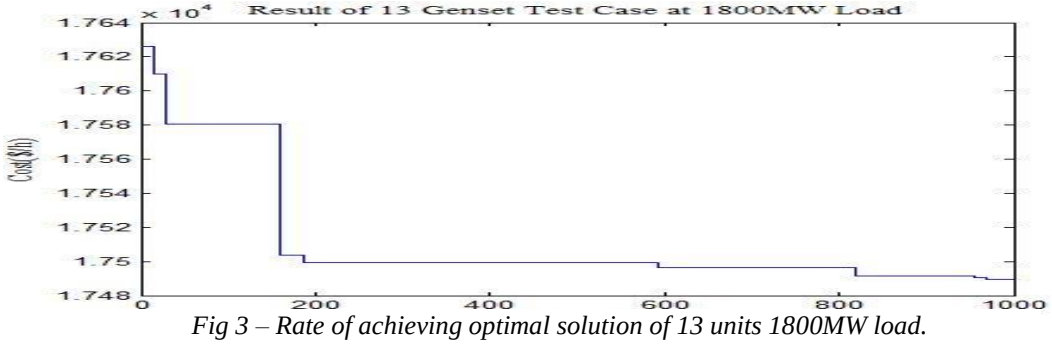

Fig 3 – Rate of achieving optimal solution of 13 units 1800MW load.

The results in Table 4. showing comparison of IGWO with SDE, MABC, PSO-TVAC, GWO and validate the superiority of IGWO in terms of cost which is the objective of paper. The cost of IGWO is 17490 ($/hr) where else have best cost ranges from 17963.879 ($/hr) to 17945.07 ($/hr). Furthermore, 455.07 ($/hr) savings leads to large scale benefit when we look it into month and year.

Table 4 – Comparison of 13 units at 1800MW load with other techniques.

Techniques	Min Cost($/hr)	Average Cost ($/hr)	Max Cost($/hr)
PSO-TVAC [6]	17963.879	-	-
MABC [5]	18127.78	18129.7010	18134.3131
SDE [7]	18134.49	18138.56	-
GWO [25]	17974.219	17994.671	18031
IGWO [22]	17945.07	17962.0	18001.0
Proposed IGWO	17490	17492.3	17493

3.2.2 Case B

In this case proposed IGWO is tested on 13 units standard test case with load 2520 MW. The valve point loading effects with other important constraints are considered. Table 5. Shows the min and max limits of the generators and the generation against each generator. The total load which is demanded 1800MW is fulfilled and the losses are 36.5MW overall at the cost of 23384 ($/hr.). Losses are considered using B coefficient method.

Table 5 – Results for 13 units with load = 2520MW.

Generator#	Pg.(min)MW	Pg.(max)MW	Output MW
1	0	680	628.5227
2	0	360	360.0000
3	0	360	360.0000
4	60	180	160.2127
5	60	180	159.8490
6	60	180	180.0000
7	60	180	169.1338
8	60	180	159.8079
9	60	180	68.7666
10	40	120	40.0000
11	40	120	120.0000
12	55	120	95.2222
13	55	120	55.0164
Demanded Load			2520 (MW)
Total Generation			2556.5 (MW)
Total Losses			36.5314 (MW)
Total Cost (\$/hr)			23384

The Fig.4. Gives the convergence characteristics for thirteen units test. It shows that the suggested algorithm converges to the most favourable point too fast and before last iteration reached.

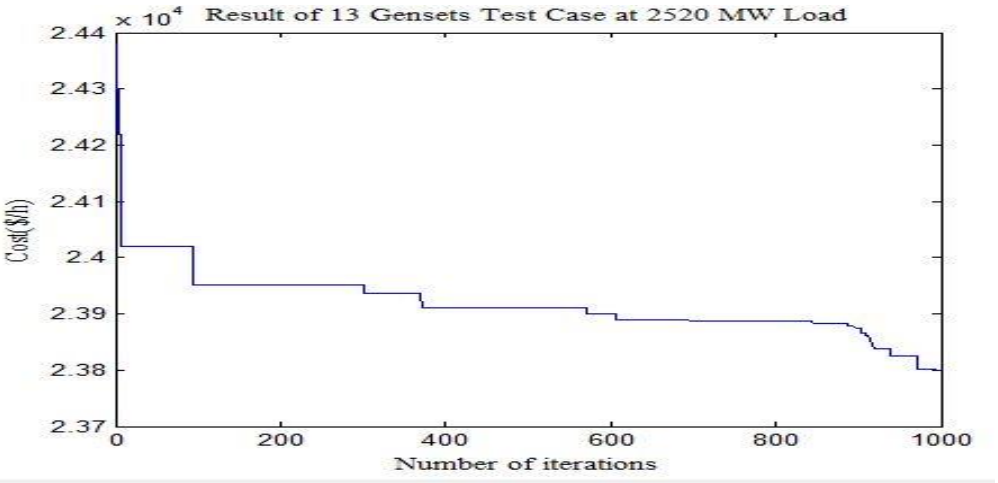

Fig 4 – Rate of achieving optimal solution of 13 units at 2520MW load.

Table 6. Provides a comparison of fuel costs. It shows the superiority of suggested algorithm in terms of minimum fuel cost. This results into saving of fuel cost when compared with DE, MABC, SDE, GWO and IGWO [22] the fuel cost savings are 24169.9177($/hr), 24514.8756 ($/hr), 24514.88 ($/hr), 24308 ($/hr) and 24202.156 respectively. The proposed IGWO gives better result as compared to above mentioned SI techniques i.e. 23384 ($/hr). Furthermore, 818 ($/hr) savings leads to large scale benefit when we look it into month and year.

Table 6 – Comparison of 13 units at 2520MW load with other techniques.

Techniques	Min Cost($/hr)	Average Cost ($/hr)	Max Cost($/hr)
DE [3]	24169.9177	-	-
MABC [24]	24514.8756	24514.8756	24514.8756
SDE [26]	24514.88	24516.31	-
GWO [19]	24308	24319	24335
IGWO[22]	24202.156	24210	24228.351
Proposed IGWO	23384	23385.3	23384.6

3.3 Test Case 03

Proposed IGWO technique is tested on 15 unit's standard test case. The demand load is 2630 MW. The VPL effect is neglected. POZ's along with transmission loss is also considered as per IEEE standards. The max number of iterations is set to 500, which is the stopping criteria and 30 numbers of wolves are considered. The Table 7. showing the min and max limits of the generators and the generation against each generator. The total load of 2630MW is fulfilled and the losses are 26.84MW overall at the cost of 32512 (\$/hr).

Table 7 – Results for 15 units with load = 2630MW.

Generator #	Pg. (min) MW	Pg. (max) MW	Output MW	Generator #	Pg. (min) MW	Pg. (max) MW	Output MW
1	150	455	455.0000	9	25	162	25.0000
2	150	455	455.0000	10	25	160	35.7380
3	20	130	130.0000	11	20	80	72.3467
4	20	130	130.0000	12	20	80	80.0000
5	150	470	233.7635	13	25	85	25.0000
6	135	460	460.0000	14	15	85	15.0000
7	135	465	465.0000	15	15	85	15.0000
8	60	300	60.0000				
Demanded Load							2630 MW
Total Generation							2656.8 MW
Total Losses							26.8482 MW
Total Cost (\$/hr)							32512.0

The Fig.5. gives the convergence characteristics for fifteen units test.. It shows that the suggested algorithm converges to the best point too fast and before last iteration reached.

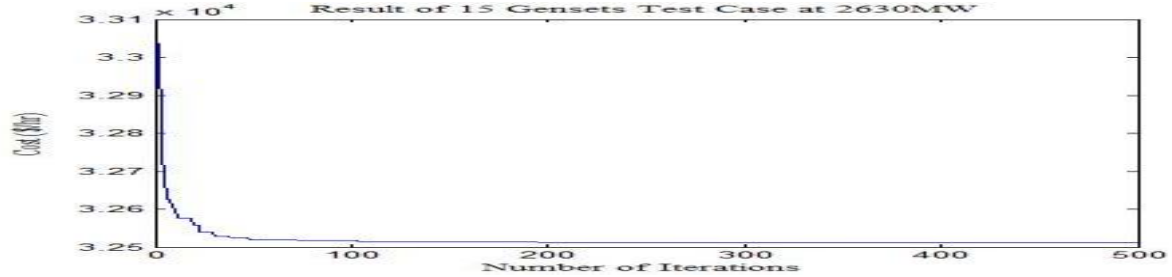

Fig 5 – Rate of achieving optimal solution of 15 units at 2630MW load.

Table 8. Showing a comparison of fuel costs and shows the superiority of proposed technique in terms of minimum fuel cost. The cost of IGWO is 32512.0 ($/hr) whereas other ranges from 32858.54 to 32550.32 ($/hr). Furthermore, 38.32 ($/hr) savings leads to large scale benefit when we look it into month and year.

Table 8 – Comparison of 15 units at 2630MW load with other techniques.

Techniques	Min Cost($/hr)	Average Cost ($/hr)	Max Cost($/hr)
IPSO [12]	32704.45	32704.45	32704.45
PSO [21]	32858.54	32989	33031
SQPSO [18]	32704.86	32707.0765	32711.6179
GAAPI [23]	32732.95	-	-
DE [3]	32609.85	32609.851	32641.419
KHA-1 [13]	32586.37	32598.0145	32592.0364
KHA-3 [13]	32564.38	32566.5782	32567.3250
GWO [19]	32555	32556.947	32558
IGWO [22]	32550.32	32552.48	32554.80
Proposed IGWO	32512.0	32512.57	32513.06

4 CONCLUSION

In this research work, proposed improved grey wolf optimization (IGWO) has been implemented for solving ED problem considering power balance constraint, generation capacity limits and transmission losses. Both linear and nonlinear ED problems have been considered in this research work. To avoid stagnation problem and premature convergence issue, mutation and crossover has been proposed is used to avoid. The proposed algorithm proves superior in terms of minimizing fuel cost as compared to Improved Grey Wolf Optimization [22] presented in 2017.

i. Fuel cost saving for first test system (06 generators) is 65 $/hr.
ii. Fuel cost saving for second test system (13 generators) with load demand =1800MW is 455 $/hr.
iii. Fuel cost saving for second test system (13 generators) with load demand = 2520MW is 818 $/hr.
iv. Fuel cost saving for third test system (15 generators) is 38.32 $/hr.

Therefore, in the light of results obtained from this research work, we conclude that proposed IGWO is an effective tool for practically to tackle the ELD problem.

5 ACKNOWLEDEGMENT

The author gratefully acknowledges the support of Muhammad Usama Malik in bringing this paper out

6 REFERENCE

[1] Sharma, Sudhir, Shivani Mehta, and Nitish Chopra. "Economic load dispatch using grey wolf optimization." International Journal of Engineering Research and Applications 5.4 (2015): 128-132.

[2] E. M. Zakria and N. M. Arbab, \Design and implementation of power system optimization using particles swarm algorithms for addressing the economic dispatch problem," International Journal of Engineering

Works Kambohwell Publisher Enterprises, vol. 4, no. 8, pp. 151{155, 2017.

[3] D. Kothari and I. Nagrath, \Modern power system analysis tata mcgraw,"2003.

[4] Aravindha babu P, Nayar KR. Economic dispatch based on optimal lambda using radial basis function network. Int J Elect Power Energy Syst 2002;24(7):551–6.

[5] Fan JY, Zhang L. Real-time economic dispatch with line flow and emission constraints using quadratic programming. IEEE Trans Power Syst 1998;13(2):320–5

[6] Dodu JC, Martin P, Merlin A, Pouget J. An optimal formulation and solution of short-range operating problems for a power system with flow constraints. IEEE Proc 1972;60(1):54–63

[7] Parikh J, Chattopadhyay D. A multi-area linear programming approach for analysis of economic operation of the Indian power system. IEEE Trans Power Syst 1996;11(1):52–8

[8] N. Singh and G. Gupta, \Grey wolf optimization technique for solving economic load dispatch problem," 2016.

[9] Ciornei and E. Kyriakides, \A ga-api solution for the economic dispatch of generation in power system operation," IEEE Transactions on power systems, vol. 27, no. 1, pp. 233{242, 2011

[10] N. Noman and H. Iba, \? constrained differential evolution for economic dispatch with valve-point effect," International Journal of Bio-Inspired Computation, vol. 3, no. 6, pp. 346{357

[11] Selvakumar and K. Thanushkodi, \Optimization using civilized swarm: solution to economic dispatch with multiple minima, "Electric Power Systems Research, vol. 79, no. 1, pp. 8{16, 2009.

[12] S. Pothiya, I. Ngamroo, and W. Kongprawechnon, \Application of multiple tabu search algorithm to solve dynamic economic dispatch considering generator constraints, "Energy Conversion and Management, vol. 49, no. 4, pp. 506{516, 2008.

[13] J.-B. Park, Y.-W. Jeong, J.-R. Shin, and K. Y. Lee, \An improved particle swarm optimization for nonconvex economic dispatch problems, "IEEE Transactions on Power Systems, vol. 25, no. 1, pp. 156{166, 2010.

[14] B. Mandal, P. K. Roy, and S. Mandal, \Economic load dispatch using krill herd algorithm, "International journal of electrical power & energy systems, vol.57, pp. 1{10, 2014.

[15] T. Sen and H. D. Mathur, \A new approach to solve economic dispatch problem using a hybrid aco {abc {hs optimization algorithm,"International Journal of Electrical Power & Energy Systems, vol. 78, pp. 735{744, 2016.

[16] M. Basu, \Kinetic gas molecule optimization for nonconvex economic dispatch problem," International Journal of Electrical Power & Energy Systems, vol. 80, pp. 325{332, 2016.

[17] Q. Niu, H. Zhang, X. Wang, K. Li, and G. W. Irwin, \A hybrid harmony search with arithmetic crossover operation for economic dispatch, "International journal of electrical power & energy

systems, vol. 62,pp.237{257,2014.

[18] M. Modiri-Delshad and N. A. Rahim, \Solving non-convex economic dispatch problem via backtracking search algorithm, "Energy,vol.77,pp. 372{381, 2014.

[19] T. Niknam, H. D. Mojarrad, and H. Z. Meymand, \Non-smooth economic dispatch computation by fuzzy and self-adaptive particle swarm optimization, " Applied Soft Computing , vol. 11, no.2 ,pp. 2805{2817, 2011.

[20] M. Pradhan, P. K. Roy, and T. Pal, \Grey wolf optimization applied to economic load dispatch problems," International Journal of Electrical Power & Energy Systems, vol. 83, pp. 325{334, 2016.

[21] S. Mirjalili, S. M. Mirjalili, and A. Lewis, \Grey wolfoptimizer ,"Advances in engineering software, vol. 69, pp. 46{61, 2014.

[22] K. Mehmood and A. Ahmad, \Improved grey wolf optimization for economic load dispatch problem considering valve point loading effect and prohibited operating zones," The Nucleus, vol. 54 no. 4, pp. 250{257,2018.

[23] D. C. Secui, \A new modified artificial bee colony algorithm for the economic dispatch problem," Energy Conversion and Management, vol. 89,pp. 43{62, 2015.

[24] S. Reddy and K. Vaisakh, \Shuffled differential evolution for large scale economic dispatch," Electric Power Systems Research, vol. 96, pp. 237{245, 2013

[25] K. T. Chaturvedi, M. Pandit, and L. Srivastava, \Particle swarm optimization with time varying acceleration coefficients for non-convex economic power dispatch," International Journal of Electrical Power & Energy Systems, vol. 31, no. 6, pp. 249

[26] Xu, Bin, et al. "Comparison between dynamic programming and genetic algorithm for hydro unit economic load dispatch." Water Science and Engineering 7.4 (2014): 420-432.

E ISSN NO. 2706-9648

Pakistan Journal of Engineering

For online access, please visit:
journal.pec.org.pk

EFFICACY OF PHOSPHORUS PENTOXIDE (P2O5) ON THE YIELD OF WHEAT USING FERTILIZER BAND DRILL IN MIXED CROP ZONE OF PUNJAB, PAKISTAN

Muhammad Ansir Muneer[1], Muhammad Yamin[2,3], Qaisar Mehmood [4], Muhammad Arshad [2]*

1 Adaptive Research Station, Faisalabad, Department of Agriculture (Ext. & A.R.), Punjab, Pakistan.
2 Faculty of Agricultural Engineering and Technology, University of Agriculture, Faisalabad, Pakistan
3Department of Biological and Agricultural Engineering, Universiti Putra Malaysia (43400) Serdang, Selangor Darul Ehsan, Malaysia.
4Department of Agriculture (Field Wing), Government of Punjab, Pakistan.

ARTICLE INFO

Article History:
Accepted on 21 April 2022
Published on 25 July 2022

Keywords

P_2O_5 fertilizer, broadcasting, fertilizer band drill, wheat grain yield, mixed crop zone.

ABSTRACT

The study pertains to the evaluation of the efficacy and assess the influence of phosphorus fertilizer on the yield of wheat. The Wheat variety "Faisalabad 2008" was used. The plot size (20 m × 15 m) of each treatment was planned in a randomized complete block design (RCBD) with total four treatments of di-ammonium phosphate as phosphorus pentoxide fertilizer (P_2O_5) application; i.e. 100% (140 kg/ha) of P_2O_5 fertilizer through broadcasting (control treatment), 100% (140 kg/ha), 75% (105 kg/ha) and 50% (70 kg/ha) of P_2O_5 fertilizer applications using fertilizer band drill with three replications. P_2O_5 fertilizer application at 100% recommended rate, i.e. (140 kg/ha) using band drill enhanced the productive tiller, 1000 grain weight and wheat yield in comparison with the other treatments but shown non-significant difference in the grain yield. Furthermore, the fertilizer band drill also saved 50% P_2O_5 fertilizer compared with the broadcasting of 100% P_2O_5 resulting in the less cost of production in the mixed crop zone of Pakistan.

NOVELTY STATEMENT: The study clearly distinguishes a better fertilizer application method through fertilizer band drill from an inefficient conventional fertilizer application method of broadcasting. It will help the farmers to efficiently utilize and save the fertilizer with the help of a fertilizer band drill.

1. INTRODUCTION

Wheat is the most important cereal crop being used by human beings as a major food component all over the world. Pakistan stands among the countries where wheat production is higher and is being cultivated over an area of 9.05 Mha and fulfils the food requirements of 45% of its population. The requirements of 30% cereal crops are fulfilled by the wheat crop globally which makes availability of 20% of overall food calories of the human body [1]. As the world population is increasing at an alarming rate, the production of wheat is a major challenge for agriculture-based countries like Pakistan. The breach between wheat production and the food requirements of the people in Pakistan is too high due to the increase in the population. This breach can be occupied by increasing the production of wheat crops per unit area. Pakistan experienced a Green Revolution in terms of higher wheat production in 1960s, but the results of this Green Revolution were not trickled to small farmers which consequently decreased the wheat production with the passage of time [2]. The global average wheat production is 3490 kg/ha, which is significantly higher than Pakistan's yield of 2940 kg/ha. Neighbouring countries (China and India) of Pakistan also have high production of wheat. In China, the production of wheat is 5480 kg/ha while India stands at 3200 kg/ha [3].

In Pakistan, there are numerous reasons for the low average production of wheat; (i) improper and excessive use of fertilizers and pesticides, (ii) non-availability of certified seed, (iii) untimely sowing and, (iv) shortage of water. Fertilizers play an essential role in wheat production. The balanced use of fertilizer not only enhances crop growth but also increases soil fertility [4]. Excessive use of fertilizer is hazardous to human health and creates environmental problems as excessive fertilizers percolate down to the subsurface and deteriorate the groundwater resources. Therefore, balanced application of fertilizer is essential for a healthy environment [5]. Crop growth and grain yield of wheat are relying on fertilizer and irrigation [6]. An excessive amount of phosphatic fertilizer amounting to PKR 4.5 billion is utilized for the sowing of wheat crop in the country. A big percentage of applied fertilizer vanishes in the soil for the reason that growing crops cannot totally consume it [7]. Correct fertilizer application is a critical component of farm management for increasing the yield of wheat [8]. The wheat production can be enhanced by the balanced usage of N and P percentages as the yield of wheat responds actively to the applied fertilizer; [4,9,10].

Further, fertilizer application technique also matters. Unlike the broadcasting technique being used in Pakistan [11], the fertilizer application in bands using fertilizer band drill saves up to 50% of fertilizer by applying 5 cm deep and 5 cm away from the wheat seed. It also increases the wheat yield by 9% compared to the broadcasting method [12]. Alam [13], concluded that the plant height, tillers per square meter and yield of wheat have expressively improved by applying fertilizer in bands. The economic analysis of the applying fertilizer in bands shows that the farmer can save up to 3250 PKR/ha using this technique [14].

Using the band drilling technique, phosphate can be positioned at the appropriate depth, therefore 60 to 70%

enhancing the efficacy of dissolved phosphorus. The application of 100 kg P_2O_5 per hectare using double fertilizer band placement has been prominent in improving the productivity of wheat crop, grain weight, 1000-grains weight and wheat grain yield [15]. Rehim et al [16] revealed that fertilizer band drill was more proficient and cost-effective than broadcasting. Hussain et al [17] summarized that application of P_2O_5 at 0.05 m far away side dressing of the plant rows at 0.05 m soil depth enhanced the plant vigour and increased the wheat grain yield under arid condition.

To evaluate the efficacy of P_2O_5 fertilizer in wheat cultivation, a comparative study was planned with the application of P_2O_5 fertilizer using a modified fertilizer band drill [18] and broadcasting technique in irrigated land of Sargodha district, Punjab, Pakistan. In this study, different percentages of P_2O_5 i.e. 100% P_2O_5 (140 kg/ha), 75% P_2O_5 (105 kg/ha) and 50% P_2O_5 (70 kg/ha) were applied using fertilizer band drill and broadcasting technique to check the effect of P_2O_5 fertilizer on wheat crop.

2. METHODOLOGY

The trial was laid out at Adaptive Research Farm, Sargodha, after the harvest of cotton in the mixed crop zone of Punjab, Pakistan. The trial aimed to evaluate the efficacy of the P_2O_5 fertilizer band drill, broadcasting and recorded their outcomes on the development and grain wheat yield. The soil of the trial location was loamy consisting of 39% sand, 31% silt and 30% clay. Soil characteristics including the organic matter, pH, EC and nutrition are shown in **Table 1**.

Table 1: Soil properties of trial site

Soil properties	Unit Value
Organic Matter	0.48(%)
Total Nitrogen	0.032(%)
Available Phosphorous (ppm)	1.94
Available Potassium (ppm)	135
pH	8.3
ECe (dSm^{-1})	1.95
Soil Texture Class	Loam

In this research trial, the wheat crop was irrigated with canal water. A plot size of 20 m × 15 m was used for each treatment. A randomized complete block design (RCBD) was employed in research trial with four treatments and three replications. Wheat variety "Faisalabad 2008" was used with Di-ammonium phosphate (DAP, 46% P_2O_5 + 18% Nitrogen) applied at the time of sowing. Wheat was sown using a drill machine after the cotton crop was harvested both years. The treatments of the trial are given in Table 2.

Table 2: Description of P_2O_5 treatments

Treatment No.	Treatment description
T_1	100% P_2O_5 (140 kg/ha) using broadcasting (control)
T_2	100% P_2O_5 (140 kg/ha) fertilizer band drill
T_3	75% P_2O_5 (105 kg/ha) fertilizer band drill
T_4	50% P_2O_5 (70 kg/ha) fertilizer band drill

The quantity of irrigation water, other agronomic and plant protection measures were identical for all the treatments. Crop data like germination rate per m^2, productive tillers per m^2, number of grains per spike, 1000 grains weight (g) and wheat grain yield (kg/ha) were recorded at the time of harvesting. The layout map of the research trial is given in Fig. 1.

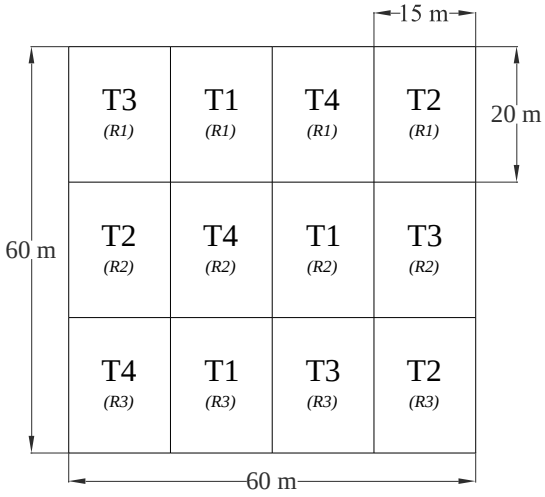

Fig. 1 Layout of research trial in RCBD experiment

3. RESULTS AND DISCUSSION

The development of germination fraction shows the capability of seeds for sprouting. In Fig. 2A, the results show that a maximum germination count of 257 per m^2 was found at 100% P_2O_5 fertilizer (140 kg/ha) application rate using a band drill which is significantly higher than 249 counts/m^2 at 100% P_2O_5 (140 kg/ha) application using broadcasting (control). Kaleem, Ansar [19)] presented the similar results. Hence, throughout the germination period, seeds did not much rely on the exterior nourishment and consumed only the composed food resources. The 50% of P_2O_5 (70 kg/ha) using fertilizer drill exhibited non-significant results in comparison with 100% P_2O_5 (140 kg/ha) using broadcasting (control) and 75% P_2O_5 (105 kg/ha) fertilizer band drill.

The data in Fig. 2B showed that P_2O_5 application using fertilizer band drill produced more tillers per m^2 i.e. 403, 391 and 376 than that of the P_2O_5 application through the broadcasting method. The highest P_2O_5 fertilizer application (140 kg/ha) using fertilizer band drill performed outclass compared with the P_2O_5 fertilizer application at 140 kg/ha using the broadcast method. These results show similar behaviour as Rahim, Ranjha [20)] and Malghani and Malik [10] presented in their studies. In a conclusion, the application of P_2O_5 using fertilizer band drill meaningfully affected the productive tillers compared to that of the broadcasting method. This outcome is in line with the finding of Turk and Tawaha [21)] who reported that the number of productive tillers per m^2 was expressively higher with fertilizer band drill compared with that of the P_2O_5 fertilizer broadcasting method.

Fig. 2C shows that the rate of fertilizer application with 100% P_2O_5 (140 kg/ha) has gained significantly more grains per spike (38.5) compared to the 75% P_2O_5 (105 kg/ha) and 50% P_2O_5 (70 kg/ha) fertilizer application using band drill. An increase in the P_2O_5 fertilizer application exhibited an improvement in growth and the grains per spike presenting the efficacy of P_2O_5 against grain development [22]; [23]. The rate of application at 100% P_2O_5 (140 kg/ha) using fertilizer band drill presented non-significant results at 38.50 average grains/spike compared to 100% P_2O_5 (140 kg/ha) application using broadcasting at 37.17 average grains/spike. The results are in line with the research of Rehim, Farooq [24)].

Fig. 2D shows that 1000 grain weight was gained more (36 g) in T_1 by 100% P_2O_5 (140 kg/ha) application using fertilizer band drill which is significantly greater than that of 32.5 g and 30.17 g with the application of 75% (105 kg/ha) and P_2O_5 50% (70 kg/ha) P_2O_5 using fertilizer band drill respectively. The results presented that a rise in the rate of P_2O_5 fertilizer is also raising the 1000 grain weight. These findings are like there results of Khan [25]. The rate of fertilizer application of 100% P_2O_5 (140 kg/ha) produced non-significantly less grain weight (29 g) using the broadcasting method compared to fertilizer band drill (36 g) resembling the findings of Rehim, Farooq [24)]. Turk and Tawaha [21)], presented the conflicting outcomes and stated that the reasonable higher 1000 grain weight was observed using fertilizer band drill compared to that of the broadcasting method.

The 100% P_2O_5 (140 kg/ha) application using a fertilizer band drill presented significantly improved results (4698 kg/ha) of grain yield compared to that of the broadcasting method (3930 kg/ha) as shown in Fig. 2E. This adequacy is due to the enhanced accessibility of phosphorous to plants using fertilizer band drill application. In the fertilizer band drill method, P_2O_5 comes into small contact with soil colloids and alkaline earth carbonates, which are moderately responsible for fixing the P_2O_5 fertilizer [20]; [26]. The recommended 100% fertilizer application rate (140 kg/ha) using band drill gained better grain yield (4698 kg/ha) which was significantly higher than that of 4355 kg/ha and 4080 kg/ha attained in 75% (105 kg/ha) of P_2O_5 and 50% (70 kg/ha) of P_2O_5 application using band drill respectively. These outcomes show similar results as presented by Hussain and Khan [17)]. The 50% (70 kg/ha) of P_2O_5 fertilizer application using band drill presented almost non-significant results compared to 100% P_2O_5 (140 kg/ha) applied through the broadcasting. These results showed that almost 50% of P_2O_5 fertilizer was saved by using the fertilizer band drill as depicted in the findings of PARC [12)].

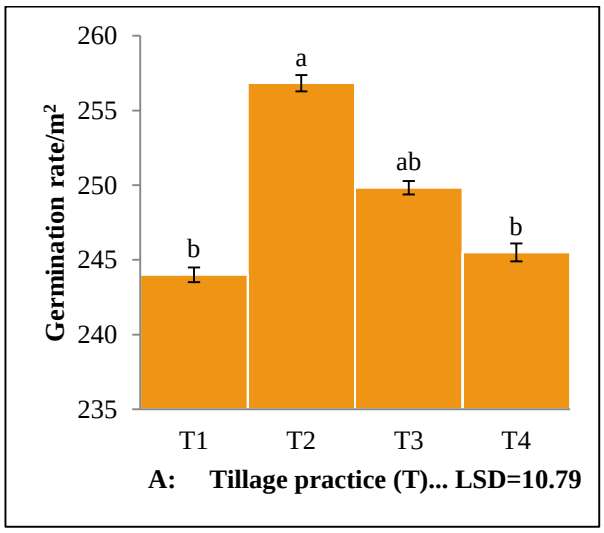

A: Tillage practice (T)... LSD=10.79

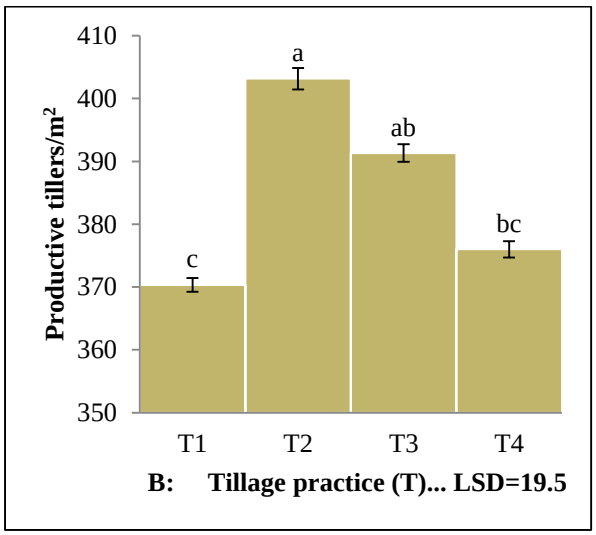

B: Tillage practice (T)... LSD=19.5

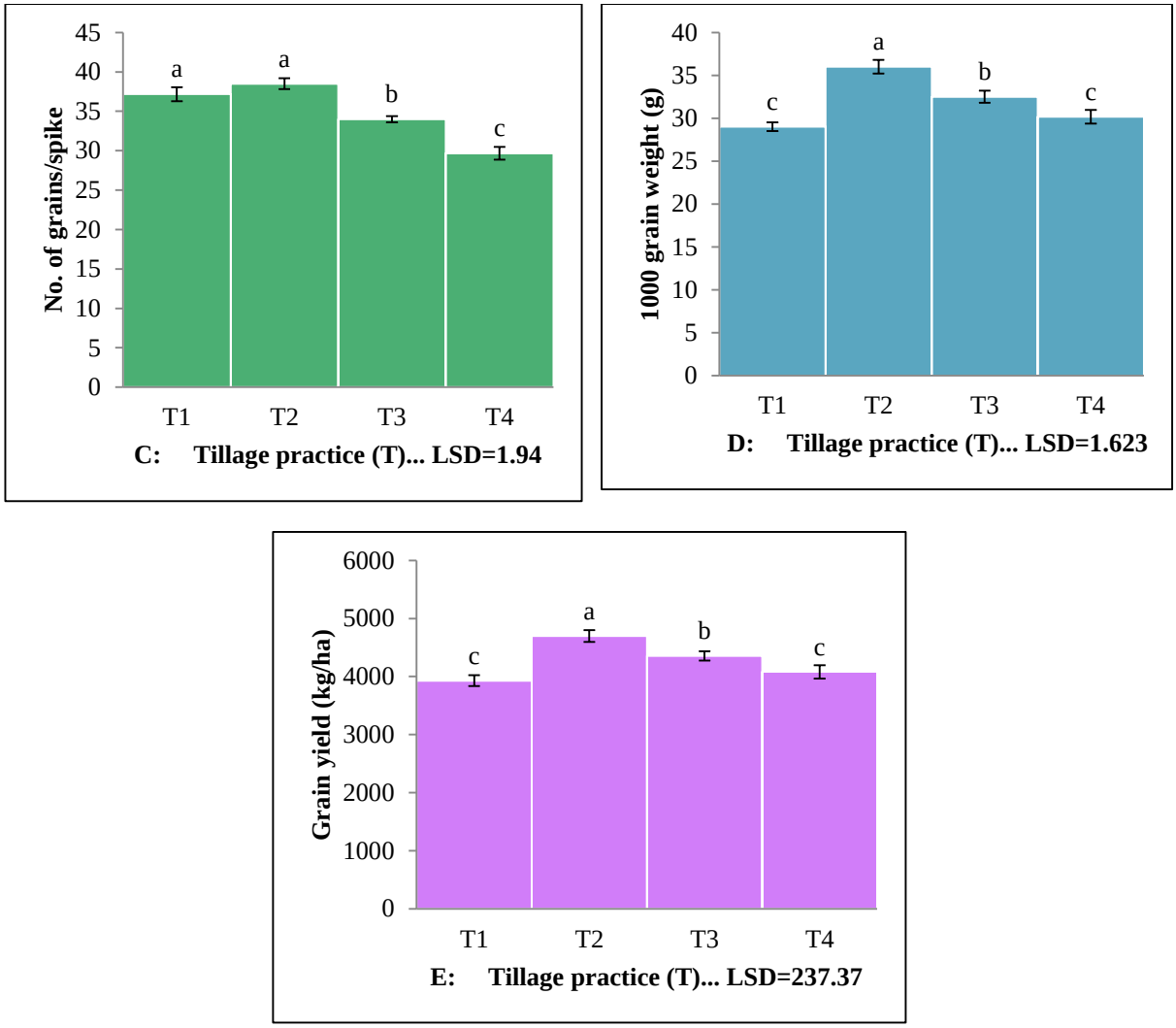

Fig. 2: Influence of fertilizer treatments on agronomic factors of wheat

4. CONCLUSION

The trial results showed that fertilizer band drill enhanced the wheat grain yield. It also improved other agricultural parameters, i.e. germination, tillers and number of grains per spike with the application of P_2O_5 fertilizer in the field. The fertilizer band drill was able to save 50% of P_2O_5 fertilizer compared to the broadcasting of P_2O_5. The non-significant results of wheat grain yield also discovered that the application rate of 50% P_2O_5 fertilizer (70 kg/ha) using fertilizer band drill is equal to 140 kg/ha which can produce meaningfully improved wheat grain yield in the mixed crop zone of Punjab, Pakistan.

5. REFERENCES

[1]. Lal R. Anthropogenic influences on world soils and implications to global food security. Advances in agronomy. 2007;93:69-93.

[2]. Abbas M, Sheikh A, Shahbaz M, Afzaal A. Food security through wheat productivity in Pakistan. Sarhad Journal of Agriculture. 2007;23(4):1239.

[3]. USDA. World Agricultural Production. United States Department of Agriculture, 2019.

[4]. Elahi E, Zhang L, Abid M, Altangerel O, Bakhsh K, Uyanga B, et al. Impact of balance use of fertilizers on wheat efficiency in cotton wheat cropping system of Pakistan. International Journal of Agriculture Innovations and Research (IJAIR). 2015;3:1369-73.

[5]. Hussain MI, Shah SH, Hussain S, Iqbal K. Growth, yield and quality response of three wheat (Triticum aestivum L.) varieties to different levels of N, P and K. International Journal of Agriculture and Biology. 2002;4(3):362-4.

[6]. Halitligil MB, Akın A, Bilgin N, Deniz Y, Öğretir K, Altınel B, et al. Effect of nitrogen fertilization on yield and nitrogen and water use efficiencies of winter wheat (durum and bread) varieties grown under conditions found in Central Anatolia. Biology and Fertility of soils. 2000;31(2):175-82.

[7]. Ali MA, Randhawa MA, Ghafoor CA, Ali L, Yamin M. Effect of phosphorus application methods on yield of wheat. Pakistan Journal of Life and Social Sciences. 2004;2(2):185-7.

[8]. El-Demardash I. Influence of nitrogen application on grain yield and end use quality in segregating generations of bread wheat (Triticum aestivum L). African Journal of Biochemistry Research. 2008;2(6):132-40.

[9]. Harbison D, Speirs A, Flavel P, Motley K, Dyson C, editors. Phosphorus—Yield responses in wheat, canola and field peas grown at different soil Colwell P and PBI levels. Proceedings 11th Australian Agronomy Conference; 2003.

[10]. Malghani AL, Malik AU, Sattar A, Hussain F, Abbas G, Hussain J. Response of growth and yield of wheat to NPK fertilizer. Sci Int(Lahore). 2010;24(2):185-9.

[11]. Malik DM, Chaudhry R, Sherazi S, editors. Management of phosphorus for wheat production in Punjab. Proc Symp On the role of phosphorus in crop production, NFDC, Islamabad Pakistan; 1992.

[12]. PARC. Fertilizer Band Placement Drill: Pakistan Agricultural Research Council (PARC); 2019 [cited 2019 Dec 17]. Available from: http://www.parc.gov.pk/files/New-Initiatives/20.pdf.

[13]. Alam S. Wheat yield and P fertilizer efficiency as influenced by rate andintegrated use of chemical and organic fertilizers. Pakistan Journal of Soil Science (Pakistan). 2003.

[14]. Ahmad M. Development and evaluation of fertilizer band placement drill for wheat. Journal of Engineering and Applied Sciences (Pakistan). 2004.

[15]. Bashir S, Anwar S, Ahmad B, Sarfraz Q, Khatk W, Islam M. Response of wheat crop to phosphorus levels and application methods. Journal of Environment and Earth Science. 2015;5(9):151-5.

[16]. Rehim A, Farooq M, Ahmad F, Hussain M. Band Placement of Phosphorus Improves the Phosphorus Use Efficiency and Wheat Productivity under Different Irrigation Regimes. International Journal of Agriculture & Biology. 2012;14(5).

[17]. Hussain S, Khan IU, Sattar A, Sher A, Ijaz M, Iqbal MM, et al. Influence of different methods and time of phosphorus fertilizer application in wheat under arid condition. J Glob Innov Agric Soc Sci. 2016;4(1):8-14.

[18]. Islam MA, Noor RS, Khan M, Ali MM, Ali Z, Mirani AA, et al. Modification and performance evaluation of fertilizer band placement drill machine for wheat crop in rain-fed areas. Pakistan Journal of Agricultural Research. 2021;34(3):417.

[19]. Kaleem S, Ansar M, Ali M, Rashid M. Effect of phoshorus on the yield and yield components of wheat variety "Inquilab-91" under rainfed conditions. Sarhad Journal of Agriculture. 2009;25(1):21-4.

[20]. Rahim A, Ranjha A, Waraich E. Effect of phosphorus application and irrigation scheduling on wheat yield and phosphorus use efficiency. Soil and Environment. 2010;29(1):15-22.

[21]. Turk M, Tawaha A. Common vetch (Vicia sativa L.) productivity as influenced by rate and method of phosphate fertilization in a Mediterranean environment. Agricoltura mediterranea. 2001;131(3-4):108-11.

[22]. Alam S, Latif A, Iqbal Z. Wheat yield and phosphorus use efficiency as influenced by method of phosphorus and zinc application. Biological Sciences-PJSIR. 2002;45(2):117-9.

[23]. Mubeen K, Wasaya A, Rehman Hu, Yasir TA, Farooq O, Imran M, et al. Integrated phosphorus nutrient sources improve wheat yield and phosphorus use efficiency under sub humid conditions. Plos one. 2021;16(10):e0255043.

[24]. Rehim A, Farooq M, Ahmad F, Hussain M. Band placement of phosphorus improves the phosphorus use efficiency and wheat productivity under different irrigation regimes. International Journal of Agriculture and Biology. 2012;14(5).

[25]. Khan R, Gurmani AR, Gurmani AH, Zia MS. Effect of phosphorus application on wheat and rice yield under wheat-rice system. Sarhad Journal of Agriculture. 2007;23(4):851.

[26]. Shah SKH, Aslam M, Khan P, Memon MY, Imtiaz M, Siddiqui S, et al. Effect of different methods and rates of phosphorus application in mungbean. Soil and Environment. 2006;25(1):55-8.

E ISSN NO. 2706-9648

Pakistan Journal of Engineering

For online access, please visit:
journal.pec.org.pk

DESIGN OF SOLAR POWERED UNMANNED AERIAL VEHICLE WITH PERPETUAL FLIGHT FOR SURVEILLANCE OF LONG-DISTANCE GAS PIPELINES

*Aun Haider *1*

[1] *College of Aeronautical Engineering*

ARTICLE INFO

Article History:
Accepted on 26 April 2022
Published on 25 July 2022

Keywords

Unmanned Aerial Vehicle, Conceptual Design, Solar Energy, Requirement Space Exploration, Design Space Exploration, Morphological Decomposition Matrix, UAV Design Analyses

ABSTRACT

The conceptual design of solar powered unmanned aerial vehicle (UAV) with perpetual flight for surveillance of long-distance gas pipelines is very much needed. The requirement of this surveillance platform has been conceived due to terrorist attacks on gas pipelines in Baluchistan. Non-consumable and regenerative nature of the fuel used in solar powered UAV makes it an eternal plane under 24/7 energy balance. Such UAV operates as a terrestrial satellite, monitoring pipelines and transmitting real time imagery to control console. The requirement space was explored to select right specification matrix for the mission profile. The 24/7 flight endurance at 15,000 ft altitude during winter solstice is the key design constraint in addition to weight and power consumption of surveillance payload. Concept space was reconnoitered through Morphological Decomposition Matrix to select tail boom arrangement with non-retractable landing gears having multiple tractor electric propulsion units. Initial sizing is done to finalize Aspect Ratio and Wing span of baseline configuration. Detailed aerodynamic, propulsion, structural, stability, performance and cost analyses of this configuration are carried out to demonstrate conformance of all design requirements.

1. INTRODUCTION

The mission of electric powered unmanned aerial vehicle (UAV) is primarily constrained by low flight endurance [1]. However, the endurance of these UAVs can be increased by utilizing solar energy, ultimately achieving virtually sustained flight for telecommunication and surveillance missions. Out of 93 solar powered aircraft built till date, only few have demonstrated flight endurance of 24 hours [2]. Nevertheless, High Altitude Long Endurance (HALE) Solar Powered

UAVs have potential for surveillance and telecommunication applications. Financial effects of design, development and operation of satellite vis-à-vis HALE UAV also approve active research in field of UAV. Furthermore, recent improvements in the efficiency of Lithium Sulphide (LiS) batteries, photo voltaic solar cells and brushless DC motors are promising [3]. Yet, a successful endeavor to harness solar energy is essential for virtually eternal flight. The potential outcomes of solar powered UAV invites exploration in aircraft design and solar propulsion systems [4]. This study presents the conceptual design of high-altitude UAV with perpetual flight to carry out the surveillance of long-distance gas pipelines in Pakistan. The presented design meets all the mission requirements within technology constraints.

2. BACKGROUND

In 1974, Sunrise I made first solar powered flight [5]. Its photovoltaic cells were installed on the top surface of wing. It weighed 27.5 lbs with 32 ft wing span. In 1980, manned solar powered aircraft Gossamer Penguin made its maiden flight. It weighed 68 lb. without pilot and had a wing span of 71 ft [6].

In 1981, US Company AeroVironment began the development of HALSOL (High-Altitude Solar Energy) UAV. This UAV led to the development of solar powered UAV weighing 486 lbs called Pathfinder [7]. It had a wing span of 98 ft and could produce 8,000 watts (W) from solar cells. In 1997, Pathfinder flew at record altitude of 71,530 ft. Later, Pathfinder was modified to develop Pathfinder Plus which flew at altitude of 80 kft. The wing span was increased to 121 ft along with installation of more efficient solar panels. The third UAV of the series was Centurion weighing 1300 lbs with a wing span of 206 ft. The fourth and last UAV of this series was Helios. It had a wing span of 247 ft with a weight of 2000 lbs. In 2001, Helios flew at an altitude of 96,500 ft. However, Helios disintegrated over Pacific Ocean during a test flight in June, 2003 [8].

In 2004, solar powered UAV Solang flew continuously for 48 hours [8]. Solang had 4 meters wingspan, 12.6 kg weight and power consumption of 65 watts (W). Solang is an impressive feat because it flew for 24 hours with solar power available during day time while remaining airborne. Solar Eagle (Vulture II) was a proposed HALE UAV developed by Boeing Phantom Works. However, this project was later cancelled in 2012.

ARCAspace® developed two solar powered medium sized UAV called Airstrato Pioneer and Airstrato Explorer, having 12 hrs and 20 hrs endurance respectively [9]. Both these UAVs can carry onboard 45 kg payload of surveillance and scientific equipment. Airstrato Pioneer carried out its maiden flight on 28 Feb, 2014.

MARRAL is a series of two solar powered UAV developed by Indian Institute of Technology (IIT) Kanpur [10]. Marral-1 is low altitude UAV with 11 hrs endurance while Marral-2 is medium altitude UAV with 18 hours endurance. Several successful test flights have been carried out starting with maiden flight on 1st Feb, 2016. The latest capitalization of solar energy is marked by the design and development of Zephyr series HALE solar powered UAV

by British company QinetiQ. 03 out of 04 Zephyr UAVs are in service. Zephyr 8 is the largest UAV of the series with a wing span of 92 ft which can carry payload of 5 kg with an endurance of 26 days.

The review of design and development history of solar powered [7] UAV reveals that few UAV have achieved 24 hours endurance only during favourable sunny weather without any power consumption of onboard surveillance capabilities. Solar powered UAV with 24/7 flight endurance will be a terrestrial satellite. Non-consumable and regenerative nature of the fuel used in this solar powered UAV makes it an eternal plane [11]. Such UAV can be used for maritime surveillance and communication capabilities.

3. AIM OF RESEARCH

The aim of this research is to present conceptual design of solar powered UAV with perpetual flight endurance which can perform 24/7 surveillance of gas pipelines in Pakistan. Detailed aerodynamic, weight, structural, performance, stability and cost analyses have been presented which substantiate conformance of UAV with design requirements.

4. CONCEPTUAL DESIGN OF SOLAR POWERED UAV

4.1 Design Requirements

A recent history [12] of attacks on gas pipelines shows that most of attacks have occurred in Sui area [13]. There are 2 air strips in this area i.e., Jacobabad and Sui. UAV must be capable to take off and land from these airstrips. After takeoff, it must climb to safe altitude of 15,000 ft and cruise to the loiter area within a range of 65 miles. UAV must have required surveillance equipment to monitor the ground activities in loiter area, data link to transmit the live imagery to ground console and flight control system. The weight and power consumption of this electronic equipment are 2 important design requirements [9]. Average payload and power consumption of COTS (Commercial of the shelf) payload is 55 lbs. and 225 watts respectively. UAV must be able to fly for 24/7 on winter solstice (i.e., 21st December) by utilizing available solar energy. UAV must harness solar energy during day time to fly and charge its onboard batteries. These onboard batteries then supply power for night flight. If UAV is able to fly on shortest day of the year i.e. 21st December for 24 hours, then it can fly around the whole year without landing [14]. This is termed as 24-hour energy balance because the solar energy available during the day must be equal to or greater than the energy used for day flight and charge batteries for overnight flight [15]. Non-consumable and regenerative nature of solar energy being utilized to power UAV implies that a solar powered UAV with 24 hours endurance on shortest day of year can fly round the year.

4.2 Conceptual Design Methodology

Conceptual design methodology presented by Noth and Siegwart [16] is suitable for initial sizing of solar powered High altitude lone endurance (HALE) UAV. It is based on 24 hours energy balance where by solar panels installed on UAV convert solar energy into electric energy during the day time. During day, available electric energy not only powers UAV but also charge onboard batteries. These batteries supply power to UAV during night when solar energy is not available.

Iterative design cycle used for initial sizing of solar powered UAV is given in Fig. . Empirical aerodynamic data for high performance sailplanes including Lift Coefficient (C_L=0.8), Drag coefficient (CD=0.015) and Oswald Efficiency (e=0.9) is utilized for initial sizing. Span (b) and Aspect Ratio (AR) are 2 design variables used to optimize the configuration of UAV [17]. In addition to these two design variables, this methodology has 2 further groups of parameters.

1. The first group of parameters is circumscribed by existing technology. These parameters when optimized for a particular application are considered as constant. Mean data of solar powered UAVs has been utilized and is given in Table 4. Invariably, increase in efficiency of electrical and mechanical components result in the decrease in total mass of UAV.
2. The second group of parameters is assumed constant for the design mission profile of UAV and is based on design requirements.

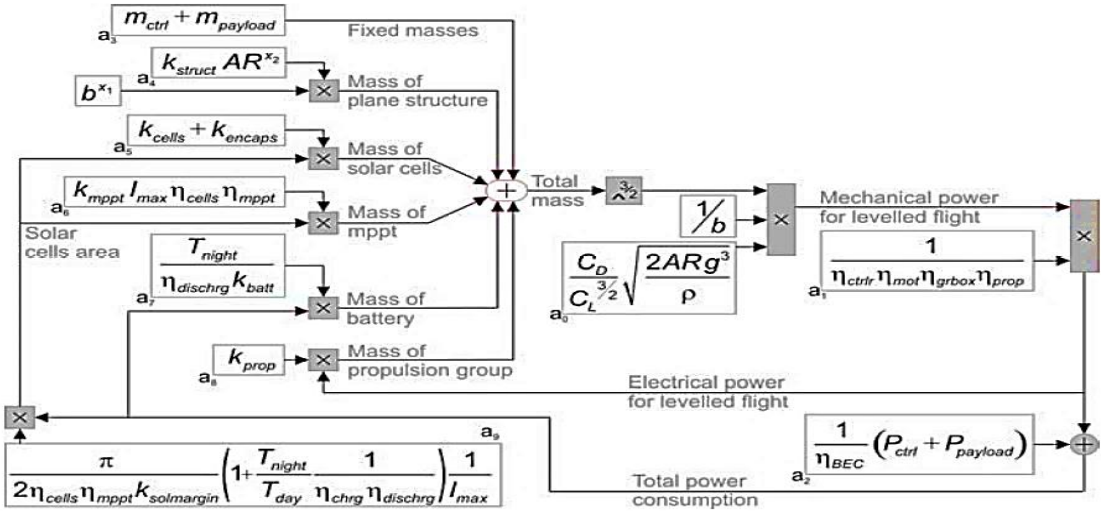

Fig. 1 Conceptual Design Methodology for Solar Powered UAV

Table 4: Efficiency of Electrical and Mechanical Components

Parameter	Value
Battery Charge/ Discharge ($\eta_{charge/discharge}$)	0.98
Efficiency Max Power Point Tracker (η_{mppt})	0.97
Efficiency Step-down Converter (η_{BEC})	0.7
Efficiency Control Servos ($\eta_{control}$)	0.95
Efficiency Solar Cells (η_{cells})	0.25

3. High altitude and long endurance solar powered UAV is similar in design and performance to sail planes [18]. Raymer Design Methodology is applicable for Sail plane design [19]. Therefore, detailed aerodynamic, structural, weight, stability, performance and cost analyses have been carried out as delineated by Raymer.

4.3 Mass Estimation Model

Total mass of UAV is the summation of masses of individual components. Therefore, a good mass model for each component is required to estimate the mass (m) of UAV [20]. Design constraints govern the mass and power consumption of payload. In addition, following heuristics

are used to estimate the mass of aircraft components [21].

1. Mass and power consumption of flight control system is estimated as 1% and 1.2% of mass ($m_{control}$) and power consumption ($P_{control}$) of UAV respectively.

2. The mass of battery is directly proportional to the energy required and inversely proportional to its energy density. The amount of electric energy stored per unit mass of the battery is defined as Battery energy density ($K_{battery}$). For LiS batteries utilized for the current application, $K_{battery}$ is taken as 350 J/kg.

3. The mass of solar panel is directly proportional to the area covered by solar panelsA_{solar}. Presently, commercially available solar panel has mass to area ratio 0.54 kg/m^2 which is sum of mass density of solar cell (k_{cell}) and encapsulation (k_{encaps}). For sustained 24 hours flight endurance, the total electric energy consumed each day is equal to the total electric energy obtained from the sun. This energy balance given in Eq. (1) provides the area of solar panels:

$$P_{electric\,tot}\left[T_{day}+\frac{T_{night}}{\eta_{charg}\eta_{discharg}}\right]=\frac{2I_{max}T_{day}K_{sol\,margin}}{\pi} \quad (1)$$

4. Maximum Power Point Tracker (*MPPT*) is an electronic device installed in solar power system which adjusts the voltage to provide maximum power. Eq. (2) gives the mass of MPPT (m_{mppt}) which is directly proportional to available solar power ($P_{sol\,max}$)

$$m_{mppt}=k_{mppt}P_{sol\,max}=k_{mppt}I_{max}\eta_{charg}\eta_{mppt}A_{sol} \quad (2)$$

Where k_{mppt} is mass to power ratio for MMPT, typically approximated as 0.00047 Kg/W

5. The mass of the propulsion group depends upon the propulsive power required and can be estimated by Eq. (3)

$$m_{prop}=K_{prop}P_{prop}=0.0045P_{prop} \quad (3)$$

6. Statistical data for high efficiency sail planes has been utilized to develop heuristics for the structural weight of HALE solar powered UAV. The structural weight of the UAV is given in Eq. (4) as a function of span (b) and aspect ratio (AR).

$$m_{struct}=b^{X1}k_{struct}AR^{X2}=b^{1.5551}*(12.31)*AR^{-0.311} \quad (4)$$

7. Total mass of UAV (m_{tot}) is sum of control system, payload, solar cells, battery, MPPT, airframe and propulsion system and is given by Eq. (5).

$$m_{tot}=m_{cntrl}+m_{payload}+m_{cell}+m_{batt}+m_{mppt}+m_{struct}+m_{prop} \quad (5)$$

4.4 Morphological Decomposition Matrix

In order to select best configuration for solar powered UAV, various alternates [22] are explored using qualitative reasoning through morphological decomposition matrix. This matrix of alternatives is given in

Table 5. Tail boom design with multiple propulsion units in a tractor configuration is selected. Selected configuration has non-

retractable landing gears to perform conventional takeoff and landing. Flexible solar panels are selected for installation on the wing. These solar panels will charge onboard high density LiS batteries.

4.5 Radiance Model

Radiance model is developed to incorporate the solar propulsion system into the design cycle by calculating the available solar energy [23]. Solar power varies with geographic location, calendar date and time of the day. 24 hours endurance on 21st December is a design constraint. Radiance model of complete year for 29.52˚ latitude is given Fig.. Available solar energy in loiter area is equal to area under the radiance curve. Maximum Irradiance (I_{max}) and available solar energy is 896 W/m^2 and 20.68 MJ/m^2 respectively.

Table 5: Morphological Decomposition Matrix

Variable	Option 1	Option 2	Option 3	Selected
Configuration	Conventional	Boom tail	Flying wing	**Boom tail**
Solar Panel Location	Wing and tail	Wing	Tracker	**Wing**
PV Type	Rigid	Flexible	--	**Flexible**
Energy source	Solar Cells	Storage batteries	Hybrid	**Hybrid**
Battery	Li Ion	LiPo	LiS	**LiS**
Landing gears	Retractable	Non retractable	N/A	**Non retractable**
Take off	Dolly launch	Rail launch	Conventional	**Conventional**
Landing	Net Arresting	Belly landing		
Propeller	Twin	Four	Multiple	**Four**
Propeller location	Pusher	Tractor	--	**Tractor**
Propeller Pitch	Fixed	Variable	--	**Variable pitch**

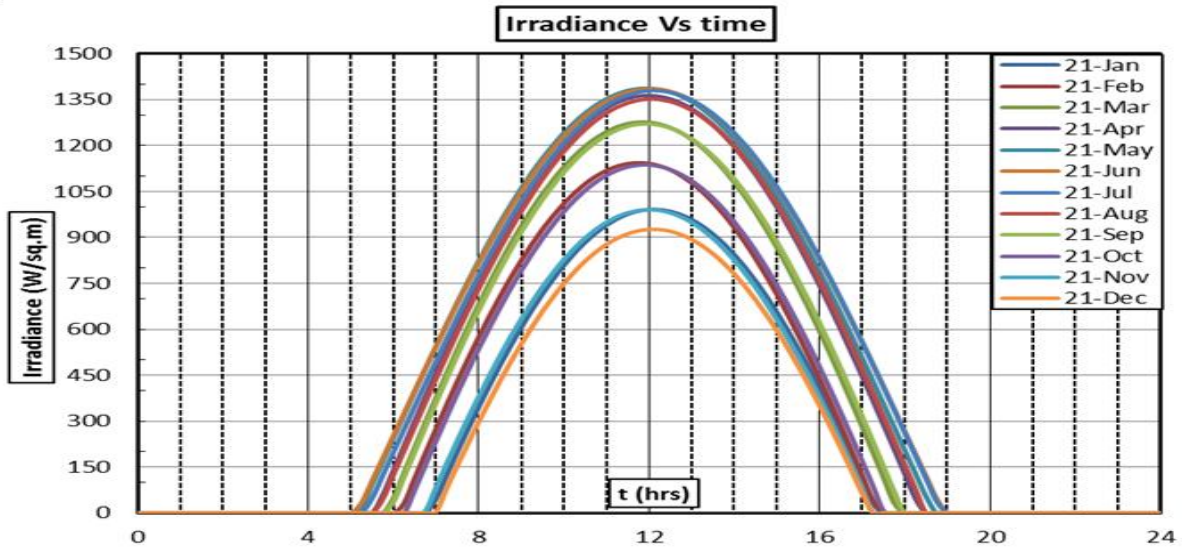

Fig.2: Irradiance Available Throughout Year

4.6 Aircraft Sizing

Based upon the design requirements, initial sizing of UAV is carried out [24]. Design of Experiments (DOE) has been carried out to explain the variation in weight of solar powered UAV due to changes in AR and span. Total 230 UAV with AR from 8 to 32 have been converged on mass and 24-hour energy balance. Fig. and Fig. relate weight and total power consumption of converged UAVs as function of AR and span. Total power consumption of UAV is sum of mechanical power consumption, electrical power consumption and energy loses including friction and heat losses. UAV with minimum weight has been selected as base line configuration. In order to improve aerodynamic performance, low Reynolds No airfoil AH94-145 with taper ratio 0.3 at mid span is selected. The selected (optimized) configuration has AR 16 with 78.8 ft span, 441 lbs weight, and reference wing area S_{ref} 388.4 ft^2. Loiter speed of the UAV is 24.34 knots with a total power consumption of 1283.5 ft. lb. /sec. Fig 3 represent the geometric view of optimized configuration.

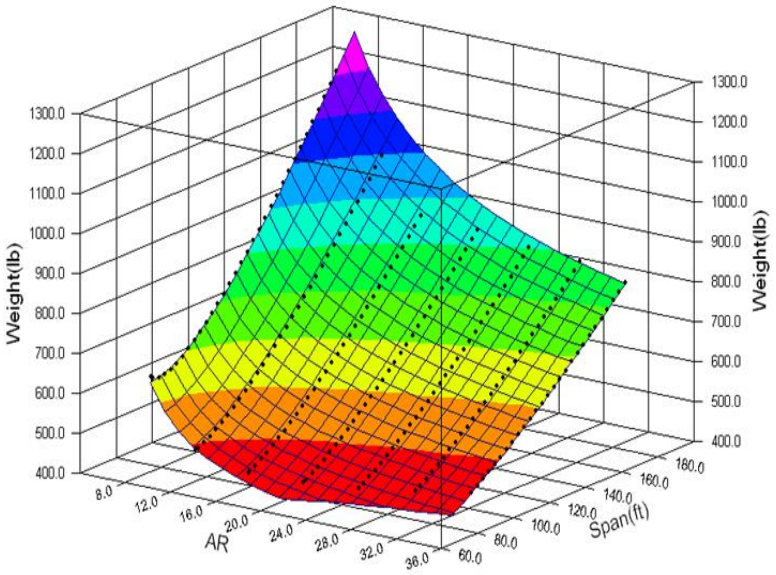

Fig.3: Weight of UAV as function of Span and Aspect Ratio

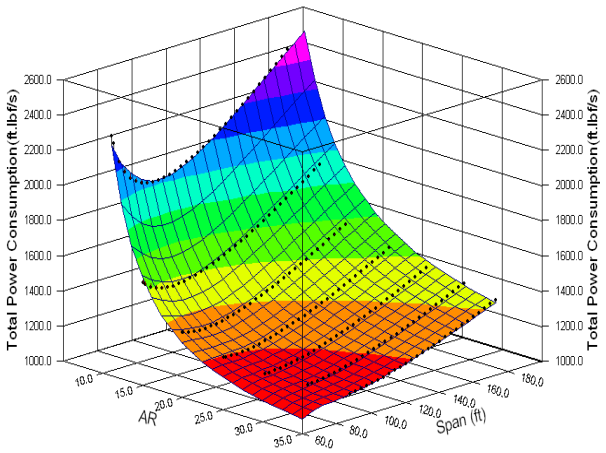

Fig.4: Power Consumption of UAV

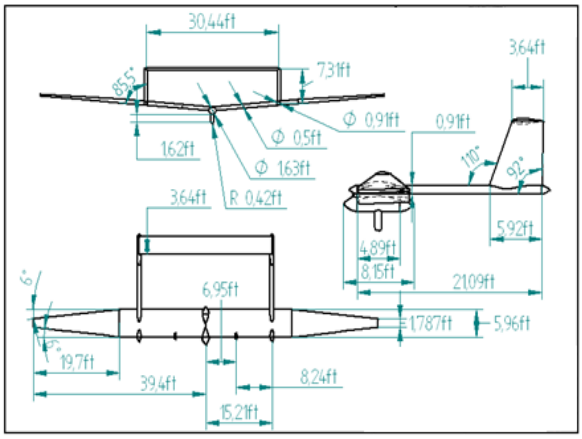

Fig. 5: Draft Model of UAV

4.7 Aerodynamic Analysis

Vortex panel method is used for aerodynamic analysis of wing, vertical and horizontal tail [25]. This method provides zero lift drag coefficient (C_{Do}) and coefficient of lift induced drug (C_{Li}) for lifting surfaces. Component build up method is used to incorporate aerodynamic effects of landing gears, fuselage, tail booms etc. In conjunction with vortex panel method, component build up method is used to determine drag polar for UAV during various flight phases. Fig. presents drag polar of UAV during takeoff, cruise and landing.

Fig.6: Drag Polar During Various Phases of Flight

4.8 Propulsion Analysis

During conceptual design phase, characteristics of propulsion system for UAV are based on historical trend [9]. In Helios and Heliplat [6], multiple brushless direct current DC motors power 2-blade variable pitch propellers through intermediary gear boxes. The same scheme has been employed through 4 Commercial off the shelf (COTS) brushless electric DC motors (Make Himax 2200-watt Ea.) to provide propulsion power (P). Diameter of each propeller (d) is estimated to be 2.38 ft using Eq. (6)

$$d(ft) = 1.83\sqrt[4]{P(hp)} \quad (6)$$

Efficiencies [3] of high performance propeller (η_{prop}=0.9), gear box ($\eta_{gear\ box}$ =0.9) and electric motors (η_{motor} =0.95) are used for calculation of available thrust (T) within flight envelop using Eq. (7). Fig 7 provides variation of available thrust (T) as function of airspeed (v).

$$P = \eta_{prop}\eta_{gear\ box}\eta_{motor}T.v \quad (7)$$

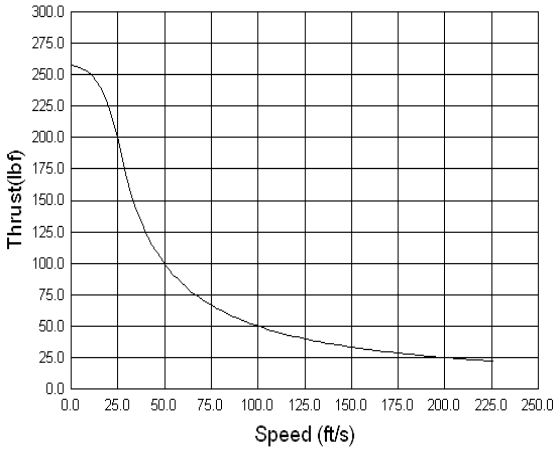

Fig.7: Variation of Thrust with Indicated Air Speed

4.9 Structural Analysis

Lift is primarily generated by wings of solar powered UAV. Resultant aerodynamic forces generate shear loads and bending moments on the wing. Fig 8 presents the span wise distribution of lift force at 3° AOA at various airspeeds. The shear force at each span station is equal to sum of lift loads outboard of that span station i.e., the integral of distributed lift load.

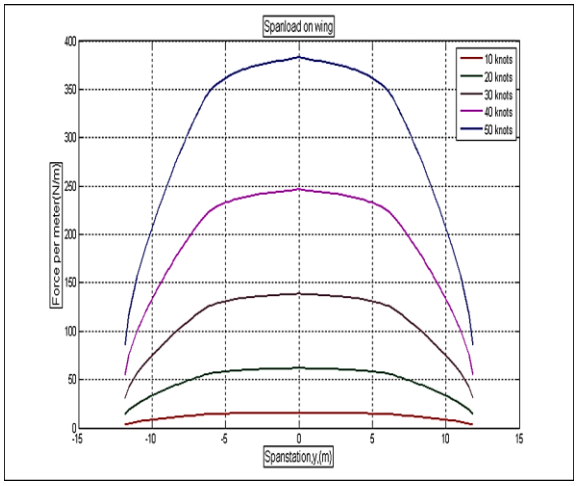

Fig.8: Span-wise Lift Distribution on Wing

Bending moment equals summation of lift loads times the distance from the span station i.e., integral of distributed lift load with respect to the distance from the span station. Fig 9 gives performance of aircraft in form of maximum load factor achieved at different velocities at 3 different altitudes within the flight envelop.

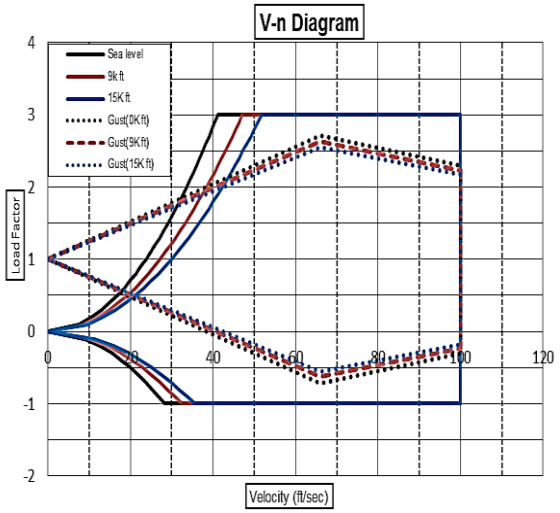

Fig.9: V-N Diagram of UAV with Gust Effect

4.10 Weight Analysis

Heuristics from Noth model [20] have been used to calculate weight of solar powered UAV. Therefore, a comparison of this UAV with solar powered UAVs and high-performance sailplanes has carried out on Great Flight Diagram in Fig.. Designed UAV falls between McCormick Boundaries defined by Eq. 8 below;

$$\frac{W}{s} = 85.5\left(W^{\frac{1}{3}} - 9.9\right) \;\&\; \frac{W}{s} = 44.8\left(W^{\frac{1}{3}} - 9.9\right)$$

Total weight of UAV is 441 lbs with reference wing area S_{ref} 388.4 ft^2. Comparison of weight and wing loading of this UAV with other solar powered UAV and sailplanes is presented in Table 6 which shows that designed UAV follows average tendency due to use of heuristics-based model.

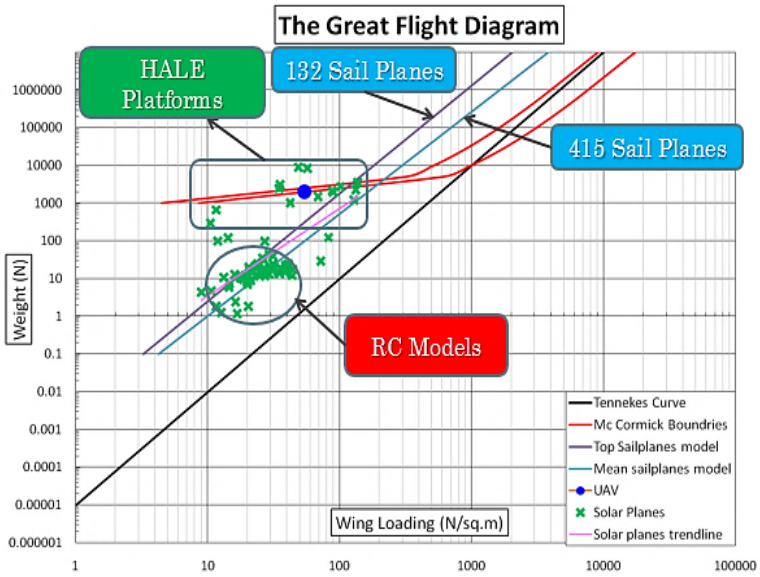

Fig.10: Weight and Wing Loading of UAV on Great Flight Diagram

Table 6: Comparison of Wing Loading with Solar Powered UAVs

UAV	Total Weight (lb)	S_{ref} (ft^2)	W/S (lb/ft^2)
Sunrazor	2050	2008	1.02
Centurion	1900	1596	1.19
Path Finder	485	263	1.83
Solair	440	236	1.86
Solar	337	234	1.43
Designed UAV	441	388	1.13

4.11 Stability Analysis

Using Raymer methodology [19], static stability analysis of solar power UAV has been carried out. The subject methodology provides step by step procedure for calculation of interceding aerodynamic and stability coefficients. The results are reported to conclude that UAV has positive static longitudinal stability ($C_{L\alpha} = 5.45/rad$) with 9.9 % Static Margin (SM), positive directional stability ($C_{m\alpha} = -0.54/rad$) and positive lateral stability ($C_{n\beta} = 0.0715/\text{rad}$).

4.12 Performance Analysis

Mechanical Power required to overcome drag force (D) for sustained flight is given by Eq. 9 below;

$$P_R = D.v = [C_D qS]\, v = [(C_{Do} + 0.02C_L^2)qS]v$$

By means of drag polar available from aerodynamic analysis, propulsive power required to overcome drag force for sustained flight at various altitudes within flight envelop has been plotted in Fig..

Radiance model provides solar power available for onboard conversion to mechanical power. This available mechanical power has been plotted as straight line on the graph for 21st December and 21st March. It is evident that mechanical power available from solar energy on 21st December is more than power required for 24 hours flight. Therefore, it validates that UAV is capable to perform 24 hours endurance throughout year on solar power only up to airspeed of 43 kts. Furthermore, total engine power available from 4 DC motors is sufficient to accelerate UAV up to speed of 100 kts. However, sustained operation at such speeds will limit flight endurance due to increased drag.

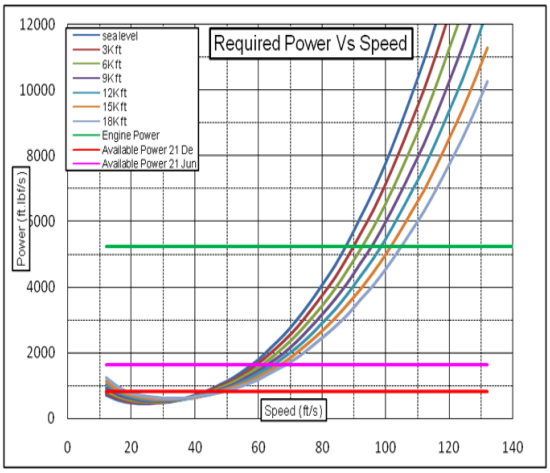

Fig.11: Available and Required Power for UAV

4.13 Cost Estimation

Rand Corporation DAPCA IV cost model [26] is used to estimate the cost of UAV during and after amortization period. This cost model is based on cost estimation relationships developed in 1986 for conventional metal aircraft. Raymer corrections [19]for inflation and composite structure of UAV have been introduced through Consumer price index (CPI) and fudge factors. Cost of UAV during and after the amortization period is given in Fig 12.

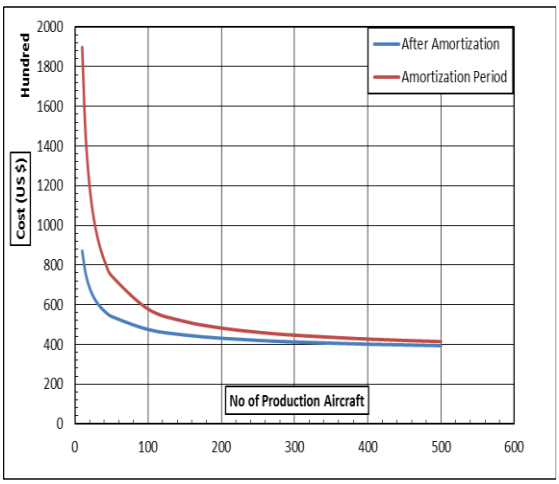

Fig. 12: Production Cost per UAV During and After Amortization Period

5 DISCUSSION ON RESULTS

In order to carry out the surveillance of gas pipelines, onboard reconnaissance equipment is required. Therefore, power consumption and weight of this equipment are the design constraints which have been incorporated in iterative design cycle. Radiance model is used to calculate maximum irradiance and available solar energy in worst case scenario i.e., 21st December. The conceptual design methodology for solar powered UAV is utilized for initial sizing of HALE platform. The 230 solar powered UAV have been converged on mass and energy balance to select a baseline configuration with minimum weight. Heuristics have been used to estimate mass of individual UAV components. Using morphological decomposition matrix, tail boom design with multiple propulsion units in a tractor arrangement is selected. The selected configuration has non-retractable landing gears to perform conventional takeoff and landing. Flexible solar panels are selected for installation on the wings. These solar panels not only provide energy for daytime flight but also charge onboard batteries. These batteries supply power to UAV during night when solar energy is not

available. This baseline configuration has been optimized with low Reynolds number Airfoil AH94-145 with taper ratio 0.3 at mid span. The solar powered UAV is capable to takeoff from landing strip at Sui or Jacobabad with on board reconnaissance equipment. It can climb to an altitude of 15,000 ft to a loiter area 62 nautical miles away and can perform 24/7 endurance flight in worst case scenario i.e., 21st December. On basis of DAPCA IV cost model, estimated cost for full scale production UAV is approx. 4.7 million PKR (USD 40,000)

6 CONCLUSION AND RECOMMENDATIONS

On the basis of the detailed analysis performed on the solar powered UAV, the following conclusions can be drawn:

1. Conceptual design methodology for solar powered UAV has been exploited successfully to design solar powered HALE platform with 24/7 endurance.

2. The feasibility of solar powered surveillance UAV is established with existing efficiency constraints of solar cells, storage batteries and composite materials.

3. All design requirement for surveillance of long-distance gas pipes with solar powered UAV have been successfully met.

4. Non-consumable and regenerative nature of the fuel used in solar powered UAV makes it an eternal plane under 24/7 energy balance. Such UAV is a cost-effective terrestrial satellite, monitoring pipelines and transmitting real time imagery to control console.

The following recommendations are made in light of analysis presented in this study:

1. Numerical analysis and wind tunnel testing of model can be performed to validate preliminary results of the conceptual design and analyses of this UAV.

2. Development of scaled down technological demonstrator is recommended to establish proof of concept.

3. The effects of wind and thermals may be studied to reduce thrust requirements of the solar powered UAV.

7 REFERENCES

[1]. Sai, L., Z. Wei, and W. Xueren. *Development Status and Key Technologies of Solar Powered Unmanned Air Vehicle*. in *IOP Conference Series: Materials Science and Engineering*. 2017. Hainan Province, China.: IOP Publishing.

[2]. Morton, S., R. D'Sa, and N. Papanikolopoulos. *Solar Powered UAV: Design and Experiments*. in *IEEE International Conference on Intelligent Robots and Systems (IROS)*. 2015. Prague, Czech Republic: IEEE.

[3]. Rajendran, P. and H. Smith. *Review of Solar and Battery Power System Development for Solar-powered Electric Unmanned Aerial Vehicles*. in *Advanced Materials Research*. 2015. Prague: Trans Tech Publ.

[4]. Hajian Maleki, M. *Conceptual Design Method for Solar powered Aircraft*. in *49th AIAA Aerospace Sciences Meeting*. 2011. West Mount, USA: CRC.

[5]. Kumar, G., S. Sepat, and S. Bansal, *Review Paper of Solar-powered UAV.* International Journal of Scientific & Engineering Research, 2015. **6**(2): p. 41-44.

[6]. Baldock, N. and M. Mokhtarzadeh-Dehghan, *A study of Solar-powered, High-altitude Unmanned Aerial Vehicles.* Aircraft Engineering and Aerospace Technology, 2006. **13**(7): p. 2147-2149.

[7]. Zhu, X., Z. Guo, and Z. Hou, *Solar-Powered Airplanes: A Historical Perspective and Future Challenges.* Progress in aerospace sciences, 2014. **71**(4): p. 36-53.

[8]. Hoffborn, M., *A Historical Survey of Solar powered Airplanes and Evaluation of it's Potential Market*. 2009, AIAA: Atlanta, Georgia. p. 127-129.

[9]. Alsahlani, A. and T. Rahulan, *Conceptual and Preliminary Design Approach of High Altitude, Long Endurance Solar-powered UAV.* CSE-PGSym, 2017. **4**(3): p. 241-243.

[10]. Dwivedi, V.S., et al. *MARAAL: A Low Altitude Long Endurance Solar-powered UAV for Surveillance and Mapping Applications*. in *2018 23rd International Conference on Methods & Models in Automation & Robotics (MMAR)*. 2018. Bombay: IEEE.

[11]. Lee, J.-S., et al. *Design of Virtual Flight System for Evaluation of Solar Powered UAV*. in *39th Annual Conference of IEEE Industrial Electronics Society*. 2013. Vienna, Austria: IEEE.

[12]. Mubin, S. and G. Mubin, *Risk Analysis for Construction and Operation of Gas Pipeline Projects in Pakistan.* Pakistan Journal of Engineering and Applied Sciences, 2016. **1**(1): p. 21-22.

[13]. Garlick, J., *Deconstructing the China–Pakistan economic corridor: pipe dreams versus geopolitical realities.* Journal of Contemporary China, 2018. **27**(112): p. 519-523.

[14]. Oettershagen, P., et al. *Perpetual Flight with a Small Solar-powered UAV: Flight Results, Performance Analysis and Model Validation*. in *2016 IEEE Aerospace Conference*. 2016. Montana, USA: IEEE.

[15]. Lee, B., et al., *Active Power Management System for Unmanned Aerial Vehicle Powered by Solar Cells.* IEEE Transactions on Aerospace and Electronic Systems, 2014. **50**(4): p. 3167-3177.

[16]. Noth, A., *Design of Solar Powered Airplanes for Continous Flight*. 2008, ETH Zurich. p. 41-44.

[17]. Van Nguyen, N., et al., *AMultidisciplinary Robust Optimisation Framework for UAV Conceptual Design.* The Aeronautical Journal, 2014. **118**(1200): p. 123-142.

[18]. Shiau, J.-K. and D.-M. Ma, *Development of an Experimental Solar-powered Unmanned Aerial Vehicle.* Journal of Chinese Institute of Engineers, 2015. **38**(6): p. 701-713.

[19]. Raymer, D., *Aircraft Design: a Conceptual Approach*. 4 ed. 2012, Reston, VA, USA: American Institute of Aeronautics and Astronautics, Inc. 141-148.

[20]. North, A., R. Siegwart, and W. Engel, *Autonomous solar UAV for Sustainable Flights*, in *Advances in Unmanned Aerial Vehicles*. 2007, Springer: ETH Zurich. p. 377-405.

[21]. Xian-Zhong, G., et al., *Parameters Determination for Concept Design of Solar-powered, High-altitude Long-endurance UAV.* Aircraft Engineering and Aerospace Technology, 2013. **12**(6): p. 214-218.

[22]. Sadraey, M.H., *Aircraft design: A Systems Engineering Approach*. 2012, New Jersey, U.S.A: John Wiley & Sons.

[23]. Rajendran, P., H. Smith, and M.H. bin Masral. *Modeling and Simulation of Solar Irradiance and Daylight Duration for a High-power-output Solar Module System*. in *Applied Mechanics and Materials*. 2014. Prague: Trans Tech Publ.

[24]. Jashnani, S., et al., *Sizing and Preliminary Hardware Testing of Solar powered UAV*. Egyptian Journal of Remote Sensing and Space Science, 2013. **16**(2): p. 189-198.

[25]. Panagiotou, P., et al., *Aerodynamic Design of a MALE UAV*. Aerospace Science and Technology, 2016. **50**: p. 127-138.

[26]. Scanlan, J., et al., *Cost Modelling for Aircraft Design Optimization.* Journal of Engineering Design, 2002. **13**(3): p. 261-269.